



UNIVERSITY OF  
BIRMINGHAM

**AN INVESTIGATION INTO COORDINATE MEASURING MACHINE TASK SPECIFIC  
MEASUREMENT UNCERTAINTY AND AUTOMATED CONFORMANCE ASSESSMENT OF  
AIRFOIL LEADING EDGE PROFILES: APPENDICES**

**By**

**HUGO MANUAEL PINTO LOBATO**

A thesis submitted to the  
**School of Metallurgy and Materials, College of Engineering and Physical Sciences,  
The University of Birmingham**

For the degree of  
**Engineering Doctorate in Engineered Materials for High Performance  
Applications in Aerospace and Related Technologies**

Structural Materials Research Centre

School of Metallurgy and Materials  
The University of Birmingham  
Birmingham  
UK

August 2011

UNIVERSITY OF  
BIRMINGHAM

**University of Birmingham Research Archive**

**e-theses repository**

This unpublished thesis/dissertation is copyright of the author and/or third parties. The intellectual property rights of the author or third parties in respect of this work are as defined by The Copyright Designs and Patents Act 1988 or as modified by any successor legislation.

Any use made of information contained in this thesis/dissertation must be in accordance with that legislation and must be properly acknowledged. Further distribution or reproduction in any format is prohibited without the permission of the copyright holder.

# Contents Listing

<b>APPENDIX 2.1 – CMM STATISTICS DATA .....</b>	<b>1</b>
<b>APPENDIX 2.3 – SENSITIVITY STUDY OF CIRCULAR FEATURES .....</b>	<b>3</b>
<b>APPENDIX 2.4 – STUDY ON THE UNCERTAINTY OF SOME INFLUENTIAL PARAMETERS IN COORDINATE MEASURING MACHINE .....</b>	<b>6</b>
ABSTRACT .....	7
INTRODUCTION .....	7
EXPERIMENTAL SET UP .....	11
RANDOMISATION ISSUES .....	14
EXPLORATORY DATA ANALYSIS .....	15
STATISTICAL MODEL .....	17
CONCLUSIONS .....	25
ACKNOWLEDGEMENTS .....	25
REFERENCES .....	26
APPENDIX .....	27
<b>APPENDIX 3 – PUNDIT/CMM EVALUATION (EXTRACTED FROM ROLLS-ROYCE 1<sup>ST</sup> YEAR ENGINEERING DOCTORATE TECHNICAL REPORT) .....</b>	<b>30</b>
INTRODUCTION .....	30
METHODOLOGY .....	31
<i>Reference values</i> .....	31
a) <i>No Variance Case</i> .....	31
b) <i>Zero case</i> .....	32
c) <i>Thermal effect case</i> .....	32
<i>Physical measurement</i> .....	33
d) <i>Analytical comparison</i> .....	34
CONCLUSIONS .....	39
REFERENCES .....	40
<b>APPENDIX 4 – AUTOMATED LEADING EDGE ASSESSMENT .....</b>	<b>41</b>
1. SOFTWARE SPECIFICATION .....	41
1.1 <i>User interface</i> .....	41
1.2 <i>Data preparation</i> .....	42
1.3 <i>Parameters</i> .....	44
1.4 <i>Configuration files</i> .....	49
1.5 <i>Bugs</i> .....	49
2. MATHEMATICAL MODELLING OF THE LEADING EDGE AND SOFTWARE TESTING .....	50
2.1 <i>Introduction</i> .....	50
2.2 <i>Blade inspect</i> .....	50
2.3 <i>Pre-Processing</i> .....	51
2.4 <i>Curve Modelling Methods</i> .....	52
2.5 <i>Curvature calculation</i> .....	57
2.6 <i>Initial Blade Inspect Testing</i> .....	59
2.7 <i>Smoothing parameters</i> .....	62
2.8 <i>Conclusions and perspectives</i> .....	65
3. CURVATURE TOLERANCING IMPLEMENTATION METHOD .....	66
3.1 <i>Introduction</i> .....	66
3.2 <i>Tolerance creation</i> .....	66
3.3 <i>Blisk assessment using tolerances in the curvature graphic</i> .....	70
4. AUTOMATION DEMONSTRATOR .....	71
4.1 <i>Introduction</i> .....	71

4.2 Automation demonstrator.....	71
4.3 Tolerance band testing on first ISR blisk (CVNTP).....	74
4.4 CVNAL vs CVNTP method for thinner blades .....	75
4.5 Conclusions.....	81
<b>APPENDIX 5 – ENGINEERING DOCTORATE CONFERENCE POSTERS .....</b>	<b>83</b>
<b>APPENDIX 6 – ENGINEERING DOCTORATE TIMELINE.....</b>	<b>85</b>

## Appendix 2.1 – CMM Statistics data

**Table 1. CMM system parameters for length bar comparison study**

<b>Machine Inputs</b>	<b>CMM-1</b>	<b>CMM-2</b>	<b>CMM-3</b>
MPE0 (ISO 10360-2)	0.6+1.5L/1000 (um)	0.8+L/400 (um)	1.2+3.3L/1000 (um)
<b>Probe</b>	<b>TP200</b>	<b>TP20</b>	<b>TP200</b>
Stdev (Unidirectional repeatability)	0.5 (um)	0.8 (um)	0.5 (um)
<b>Environment (Average Temperature)</b>	<b>20.514 (C)</b>	<b>20.662 (C)</b>	<b>20.004 (C)</b>
Stdev (Temperature)	0.069 (C)	0.2 (C)	0.397 (C)
Scales	Zerodour	Glass	Glass
CTE	0.15 ppm/C	8.33 ppm/C	8.33 ppm/C
UCTE	0.015	0.833	0.833
<b>Length Bars</b>	<b>Step (Gauge Steel)</b>	<b>Step (Gauge Steel)</b>	<b>Koba Gauge (Steel)</b>
Calibration Uncertainty	0.12+0.0017L (um)	0.00007*L <sup>2</sup> -0.00002*L+0.00003 (um)	
CTE	11.8 ppm/C	11.8 ppm/C	11.5 ppm/C
U	1.18	1.18	1.15

**Table 2. CMM-3 measurement data**

<b>Nominal</b>	20.001	99.9949	220.018	300.0091	420.0021
<b>Run 1</b>	20.0014	99.9955	220.0194	300.0105	420.004
<b>Run 2</b>	20.0012	99.9954	220.0192	300.0106	420.004
<b>Run 3</b>	20.0015	99.9954	220.0193	300.0107	420.0039

**Table 3. CM-2 measurement data**

<b>Nominal</b>	20.0008	100.0232	220.0322	300.0564	420.0494	500.0463
<b>Run 1</b>	20.0007	100.0229	220.0317	300.0563	420.0494	500.0462
<b>Run 2</b>	20.0006	100.0228	220.0316	300.0562	420.0493	500.046
<b>Run 3</b>	20.0005	100.0227	220.0315	300.0561	420.0492	500.0459
<b>Run 4</b>	20.0008	100.0232	220.0326	300.057	420.0501	500.0464
<b>Run 5</b>	20.0008	100.0231	220.0325	300.057	420.0501	500.0464
<b>Run 6</b>	20.0009	100.0234	220.0327	300.0573	420.0503	500.0466
<b>Run 7</b>	20.0009	100.0235	220.0323	300.0566	420.0498	500.0464
<b>Run 8</b>	20.0009	100.0234	220.0323	300.0566	420.0497	500.0464
<b>Run 9</b>	20.0009	100.0234	220.0323	300.0566	420.0498	500.0464
<b>Run 10</b>	20.0005	100.0233	220.0325	300.0568	420.0495	500.0456
<b>Run 11</b>	20.0004	100.0232	220.0324	300.0568	420.0493	500.0456
<b>Run 12</b>	20.0005	100.0233	220.0324	300.0568	420.0494	500.0455

**Table 4. CMM-1 measurement data**

<b>Nominal (mm)</b>	<b>30.000500</b>	<b>110.000600</b>	<b>410.000200</b>	<b>609.999900</b>	<b>809.999500</b>
<b>Run 1</b>	29.999900	110.000100	410.000900	610.000900	810.000900
<b>Run 2</b>	30.000200	110.000500	410.001200	610.001200	810.001000
<b>Run 3</b>	30.000200	110.000500	410.001100	610.001100	810.000800
<b>Run 4</b>	30.000000	110.000300	410.000300	610.000800	810.000900
<b>Run 5</b>	29.999900	110.000300	410.000600	610.000500	810.001100
<b>Run 6</b>	30.000100	110.000400	410.000300	610.000200	810.000800

## Appendix 2.3 – Sensitivity study of Circular Features

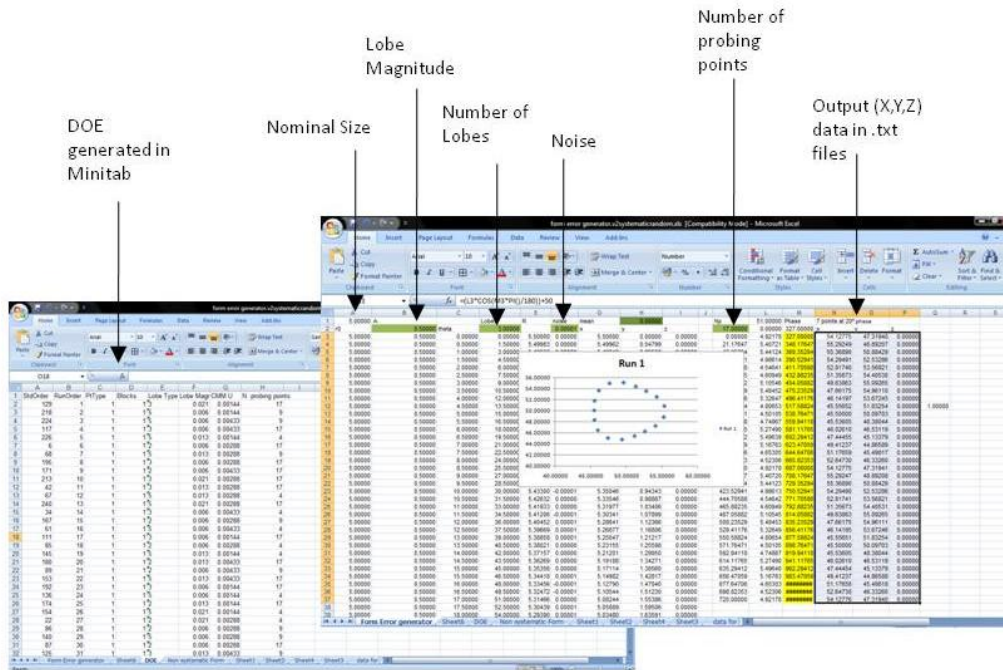


Figure 1. Excel User interface for Monte Carlo model for circular features

```

Microsoft Visual Basic - form error generator.v2systematicrandom.xls - [Module1 (Code)]
File Edit View Insert Format Debug Run Tools Add-Ins Window Help
Type a question for help
Project - VBAProject
Sheet2 (DOE)
Sheet3 (Non syst)
Sheet4 (Sheet1)
Sheet5 (Sheet2)
Sheet6 (Sheet2)
Sheet7 (Sheet4)
Sheet8 (Sheet3)
Sheet9 (data for
ThisWorkbook
Forms
Modules
Module1
Properties - Module1
Module1 Module
Alphabetic Categorized
(Name) Module1
Watches

Sub WriteXY(cycles As Integer, points As Integer, prefix As String, dir As Integer)
Application.ScreenUpdating = False
MkDir "C:\Users\My Computer\Documents\EngD\Measurement Uncertainty\Sensitivity study\" & Str(dir)
For i = 1 To cycles
Open "C:\Users\My Computer\Documents\EngD\Measurement Uncertainty\Sensitivity study\" & Str(dir) & "\" & prefix & i & ".txt" For C
Sheets("Form Error generator").Activate
Range("N3:O" & points + 2).Copy
Sheets("Sheet1").Activate
Range("A1").PasteSpecial xlPasteValues
For j = 1 To points
x = Range("A" & j)
y = Range("B" & j)
Print #1, x & ", " & y & ", " & 0
Next j
Range("A1:Z100").Clear
Close #1
Next i
Application.ScreenUpdating = True
End Sub

Sub Run()
For i = 2 To 244
Sheets("DOE").Activate
D2 = Range("E" & i)
B2 = Range("F" & i)
F2 = Range("G" & i)
K2 = Range("H" & i)
Sheets("Form Error generator").Activate
Range("D2") = D2
Range("B2") = B2
Range("F2") = F2
Range("K2") = K2
Module1.WriteXY 1000, Val(K2), "run", i - 1
Next i
End Sub

```

Figure 2. Excel Macro of the Monte Carlo model.

Feature size mean error

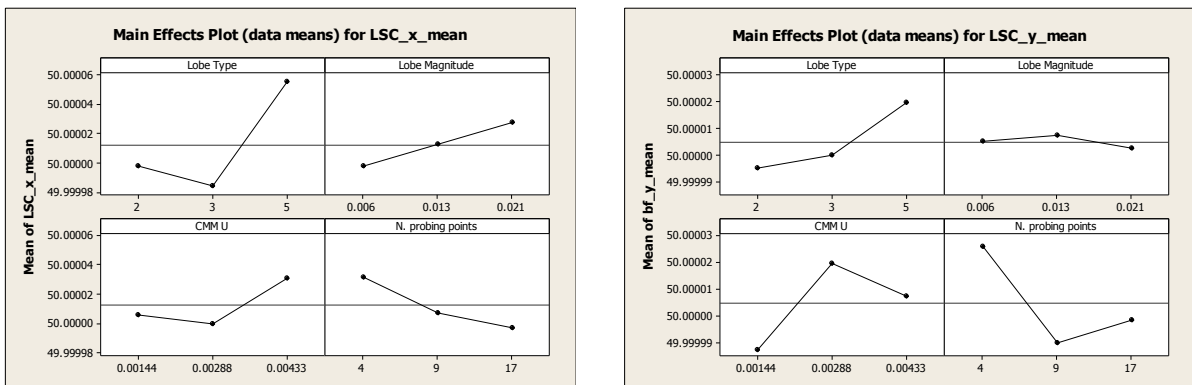


Figure 3. Main effects plots for the LSC centre coordinates mean error



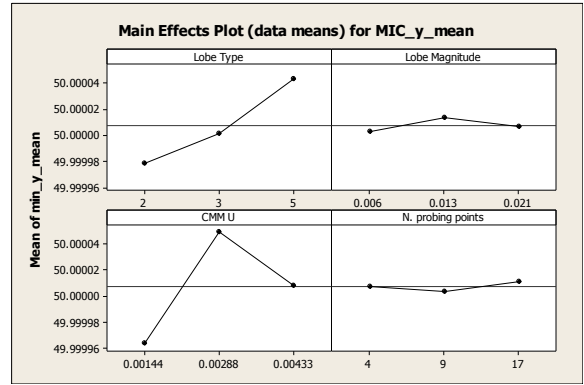
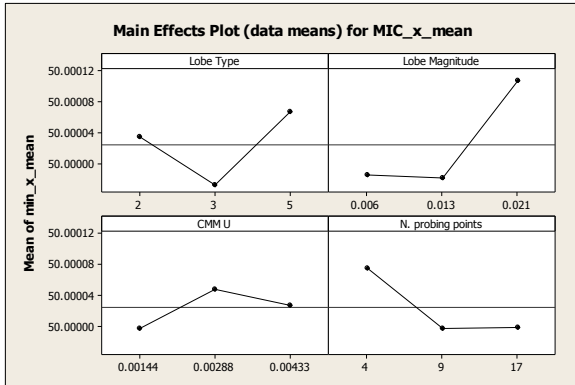


Figure 4. Main effects plots for the MIC centre coordinates mean error

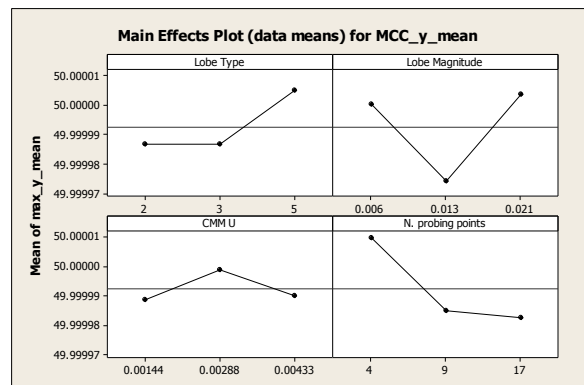
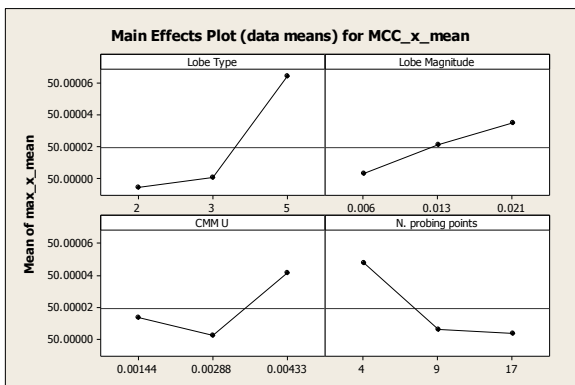


Figure 5. Main effects plots for the MCC centre coordinates mean error

Feature size stdev

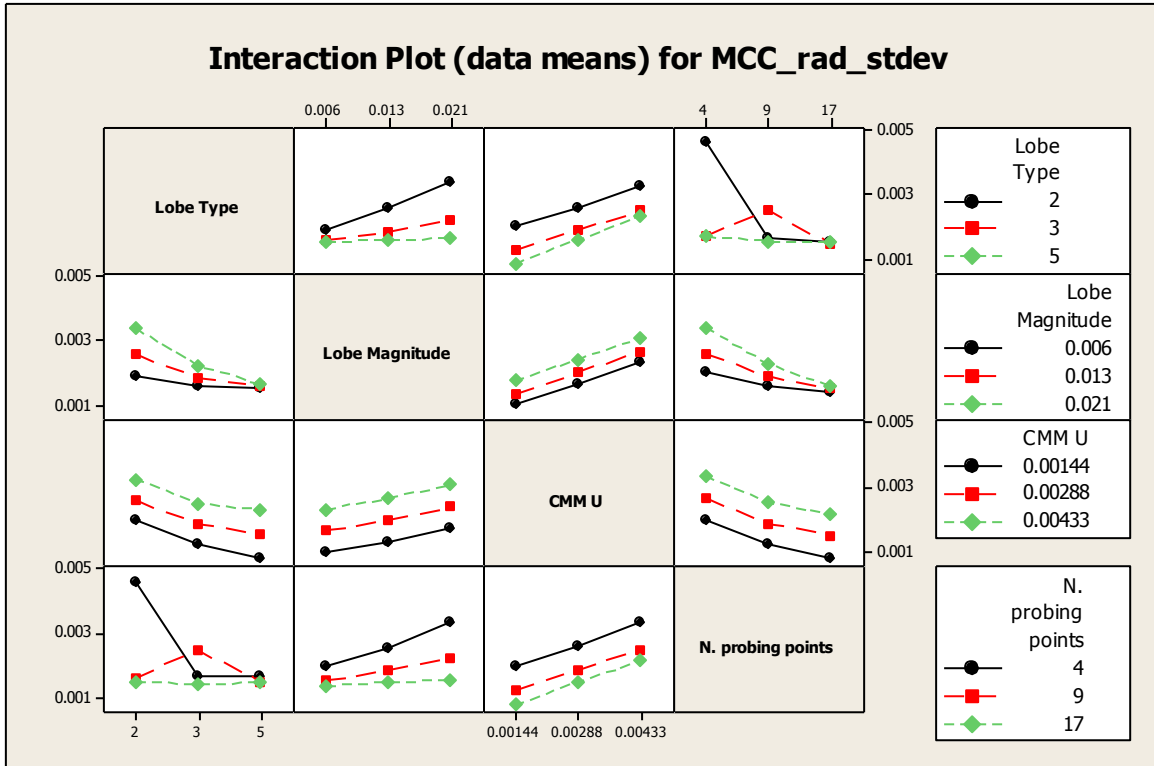


Figure 6. Interaction plot for the feature size MCC standard deviation.

## Appendix 2.4 - Study on the uncertainty of some influential parameters in coordinate measuring machine

# STUDY ON THE UNCERTAINTY OF SOME INFLUENTIAL PARAMETERS IN COORDINATE MEASURING MACHINE

**Hugo Lobato<sup>a</sup>, Carlo Ferri<sup>b</sup>, Julian Faraway<sup>c</sup>, Nick Orchard<sup>a</sup>**

<sup>a</sup> Rolls-Royce plc, P.O. box 31, Derby DE24 8BJ, UK

<sup>b</sup> University of Bath, Mechanical Engineering Dept., Quarry Road, Bath, BA2 7AY, UK

<sup>c</sup> University of Bath, Mathematical Sciences Dept., Quarry Road, Bath, BA2 7AY, UK

## Abstract

Any measurement method of a physical quantity cannot provide an exact unequivocal result due to the infinite amount of information necessary to characterise fully both the physical quantity to be measured and the measuring process. A quantitative indication of the quality of a measurement result needs therefore to be given to enable its reliable use. Uncertainty is one such indication. Provision of incorrect uncertainty statements for measurements performed by a coordinate measuring machine (CMM) may lead to very serious economic implications. In this study, the uncertainty of CMM measurements is estimated by a single parameter accounting for both systematic and random errors. The effects that environmental conditions (temperature), discretionary set-up parameters (probe extension, stylus length) and measuring plan decisions (number of points) have on uncertainty of measurements is then investigated. Interactions between such factors were also shown to be significant.

## Introduction

During the last two decades coordinate measurement systems (CMS) have been assuming an increasingly predominant role in the verification of compliance to dimensional and geometrical specifications of manufactured parts in a number of industries (for instance aerospace and biomedical). The distinct advantage of coordinate measuring machines (CMM) over other inspection systems is their intrinsic versatility. This enables them to be deployed in a large variety of measurement tasks which are often very demanding.

Three standards are commonly used by CMM manufacturers to specify the performances of their machines, namely the ISO 10360-1:2001 [1], the ASME B.89 [2] and the VDI/VDE [3].

Measurements taken according to these standards tend to involve artefacts such as step gauges, length bars and gauge blocks. These produce an estimate of the machine performance in terms of a volumetric measuring uncertainty value also known as maximum permissible error (MPE).

Regardless of the standard method used, the evaluation of the machine specification is fully trustworthy only for the set of conditions under which the evaluation took place. The term “conditions” refers to all those factors that may have an effect on the measurement result. These factors could be the different types of probes (e.g. kinematic or piezoelectric), accessories (e.g. styli or probe extension), machine settings (e.g. measurement speed or measurement acceleration), sampling strategy (e.g. number of points and distribution [15]) and environment (e.g. temperature or vibration). Some of these factors may affect a measurement result only in terms of systematic error, others in terms of random error and others again in terms of both. In the “International Vocabulary of Basic and General Terms in Metrology” [4], also known as VIM and published by the International Organisation for Standardisation (ISO), Systematic error is defined as “mean that would result from an infinite number of measurements of the same measurand carried out under repeatability conditions minus a true value of the measurand” [4]. The mean referred to in this definition is represented as  $\bar{x}_\infty$  in Figure 1. Random error, on the other hand, is the “result of a measurement minus the mean that would result from an infinite number of measurements of the same measurand carried out under repeatability conditions” [4]. The term result mentioned above is represent as  $\bar{x}$  in Figure 1. In practice, neither can be known exactly but must be estimated. Error without any further specification is the sum of the systematic and the random error [4]. The term measurand refers to the quantity to be measured (e.g. the thickness of a metal sheet at a specified temperature), whereas true value (or simply value) of a measurand refers to that ideal value that completely fulfils the specification of the measurand (cf. annex D in [5]). Error,  $e$ , systematic error,  $e_s$ , random error,  $e_r$  and true value  $\theta$  are illustrated in Figure 1.

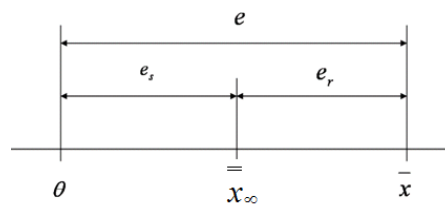


**Figure 1 Interpretation and relationship between error, systematic error and random error.**

Errors in CMM's have been grouped by Hermann et al. [6] in three categories:

- 1-Geometric errors due to the individual machine components (e.g. scales, axes' motors).
- 2- Errors related to the stiffness of structural machine components (e.g. Z ram, bridge).
- 3- Errors due to thermal effects (internal or external).

For the systematic error, some of the factors having a significant effect on a CMM machine have been identified by Feng and Pandley [7].

For the random error, a number of factors significantly affecting a CMM while measuring circular features have been identified by Feng [8]. Miguel and Cauchick [9] demonstrated a technique for evaluating CMM touch trigger probes using a motorised traversing table coupled with a laser interferometer. The authors demonstrated how the random error of the probe head varied with the indexing angle and the stylus length.

A first objective of this investigation is to provide a single performance parameter that jointly accounts for both systematic and random errors of a coordinate measuring machine. However, characterizing the concept of error, both systematic and random using estimation procedures founded on experimental activities and subsequent statistical analyses of the results does not enable the investigator to reach conclusions that are certain. A doubt about how adequately a measurement result represents the value of the quantity undergoing measurement is apparent (cf. section 0.2 in [5]).

To account for this impossibility of reaching conclusions that cannot be doubted, the concept of uncertainty was introduced and detailed in the "Guide to the expression of uncertainty in measurement" (GUM) published by ISO [5]. Adopting this perspective, thereafter the term uncertainty is preferred to the term error. In the GUM [5], the word uncertainty conveys two different meanings. The first is the generic concept of "doubt about the validity of the result of a measurement". The second is the specific concept of "parameter, associated with the result of a measurement that characterizes the dispersion of the values that could reasonably be attributed to the measurand".

The specific concept will be used throughout this investigation unless otherwise stated. The root mean squared error, *rmse*, has been selected as the parameter mentioned in the

uncertainty definition. Such a quantity represents the dispersion of a series of  $n$  measurement results,  $\bar{x}_i$ , from the value of the measurand,  $\theta$ , namely:

$$rmse(\bar{x}_i, \theta, n) = \sqrt{\frac{\sum_{i=1}^n (\bar{x}_i - \theta)^2}{n}} \quad (1)$$

In equation 1 the measurement result of the  $i$ -th measurement task is represented with  $\bar{x}_i$  to denote the fact that in this study it has been computed using the average of three test results performed in repeatability conditions (cf. section 3.6 in the VIM [4] for a definition of repeatability conditions). This is equivalent to saying that a measurement task encompasses three measurement tests. The  $rmse$  is expressed in the same unit as the measurement result and the value of the measurand (e.g. metres for a length).

Equation 1 can then be rearranged to  $rmse(\bar{x}_i, \theta, n) = \sqrt{\frac{\sum_{i=1}^n (\bar{x}_i - \bar{x})^2}{n} + \frac{\sum_{i=1}^n (\bar{x} - \theta)^2}{n}}$ , which

shows that  $rmse$  is given by the square root of two additive terms (further detail can be found for instance in [10]). The first term is the square of the bias, which accounts for the systematic error. The second term is the sample variance that represents the dispersion of the series of measurements about their mean and that therefore expresses the random error. These considerations enable the selected uncertainty parameter to be identified as completely fulfilling the first objective of this study. They also reveal the existence of some similarities between the approach based on  $rmse$  presented in this investigation and the method for determining the uncertainty of measurement illustrated in the technical specification ISO/TS 15530-3 [11].

A second objective of this investigation, is the identification of experimental conditions (i.e. environment, probe extension) that may significantly affect the  $rmse$  and that are likely to be encountered in the large variety of measurement tasks that the machine can perform. It is believed that pursuing this second objective may contribute to raising the awareness of the practitioners regarding the detrimental effect that uncontrolled or uncontrollable experimental conditions may exert on the machine specification. Moreover, it enables set-up parameters to be chosen so that the resulting uncertainty of measurement quantified by  $rmse$  is lower. *Such information is vital for decisions associated with CMM inspection planning [16].* The method presented in this study can then be adapted to suit the specific

environment conditions and needs of the measurement tasks of interest to a specific organisation.

## Experimental set up

A commercially available CMM was used for the experimental study. The machine was a moving bridge with a specification  $MPE=(3.5+L/250)\mu\text{m}$  (L being a length in mm) according to ISO 10360-1:2001 [1]. The experimental set-up is shown in Figure 2.

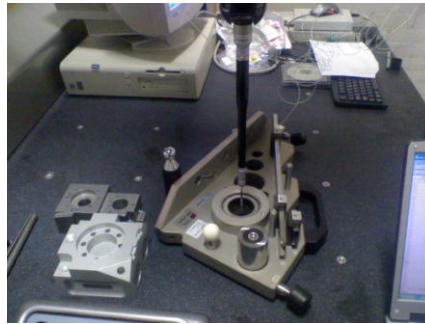


**Figure 2 Experimental set-up.**

The machine was located in a temperature controlled room where the temperature can be set at a pre-specified reference value within an uncertainty of  $\pm 1\text{ }^{\circ}\text{C}$  at 95 % significance level. Therefore, by setting different levels of room temperature it is possible to simulate measurement tasks performed in workshop environments where the temperature may vary considerably throughout a working day during normal operating conditions. In environments that lack temperature control, the temperature is an uncontrolled nuisance factor, whose effects on the uncertainty of measurement expressed in terms of *rmse* it is believed sensible to investigate.

In this investigation, two levels of room temperature were selected, 21 and 24 $^{\circ}\text{C}$ , respectively, and no temperature compensation settings were enabled on the CMM throughout the whole experimental activity. The stability of the machine temperature at each of the two levels of air temperature considered was monitored using K type thermocouples applied in a number of points of the machine.

Another factor that may have a significant effect on the uncertainty of measurement of a CMM is the geometric characteristic (form and dimensions) of the parts to be measured. In fact, performing a measurement task on parts with different dimensions engages each of the axes of motion of the CMM in different ways. Moreover, the extension of motion of each of them is expected to be different. Similar considerations apply for parts of comparable dimensions but with different form. To represent the variety of parts that have different geometrical characteristics and that can be measured using a CMM, two different features were selected for this study: a ring gauge (R) and a sphere (S) to represent two and three dimensional features, respectively. In both cases, the measurand was defined as the diameter of the part at each of the two examined levels of air temperature. As shown in equation 1 the *rmse* is also a function of the value of the measurand,  $\theta$ , that cannot be completely known because the measurand itself cannot be completely identified without an infinite amount of information (cf. section D1.1 in the GUM [5]). Therefore an estimate of  $\theta$ , i.e.  $\hat{\theta}$ , is needed in order to have an estimate of the *rmse*, i.e.  $\hat{rmse}$ . By using a certified reference material (CRM, cf. section 6.14 in the VIM [4] for a definition) encompassing both a ring gauge and a sphere, not only is it possible to have an estimate of the value of the measurand, i.e.  $\hat{\theta}$ , accompanied by a standard uncertainty value (cf. section 2.3.1 in the GUM [5] for a definition), but also traceability to the official realisation of the unit of measurement of the measurand is established. That is, for CRM of length, an official realisation of the definition of the metre.

These characteristics of a CRM are summarised in a document called a calibration certificate. Notwithstanding, the values of both the measurands provided in this document are valid at a reference temperature  $T_{ref}$  that is also stated in the certificate. For the measurand in this study, as is typical with any length,  $T_{ref} = 20^{\circ}\text{C}$ . Thermal expansion for the sphere (external feature) and thermal contraction for the ring gauge (internal feature) is expected to affect the values provided by the certificate when the operating temperature of the CRM is higher than  $T_{ref}$ , as in this study. Consequently, new estimates  $\hat{\theta}_T$ 's for the values of the measurands valid when the temperature of the measurand is  $T$  were produced using the following equation, under the assumption of linear thermal expansion of the CRM:

$$\hat{\theta}_T = \hat{\theta} + \alpha_{T_{ref}} \cdot (T - T_{ref}) \cdot \hat{\theta} \quad (2)$$

In equation 2  $\alpha_{T_{ref}}$  is the coefficient of linear thermal expansion when the CRM is at the temperature  $T_{ref}$ . The temperature  $T$  of the CRM when the air temperature was set at 21 and 24 °C respectively, was monitored attaching K type thermocouples to the CRM at a



number of points. The average of these measured values of temperature was used in equation 2. Some of the information available on the calibration certificate of the CRM used have been summarised in Table 1.

FEATURE	CALIBRATED VALUE (mm)	UNCERTAINTY (mm)	COEFFICIENT OF THERMAL EXPANSION (pp/mC)
Ring Gauge	49.9994	0.4	11.5
Sphere	29.9992	0.4	5.5

**Table 1. Features calibration data**

Ultimately, an estimate  $\hat{rmse}$  of a series of measurement results taken in the  $i$ -th experimental condition is obtained using  $\hat{\theta}_T$  from equation 2. The series of measurements has been taken in repeatability conditions. The results  $\bar{x}_i$  and  $\bar{x}_{i+1}$  have not been obtained one after the other in a temporal sequence, but have been assigned to the run order by randomly selecting them from all the measurements in all the investigated experimental conditions at a pre-specified temperature. Differently stated, the measurements results are replicates and not repetitions of the measurement process.

When setting up a CMM for a specific already assigned measurement task, it often appears that the operator may be left with some discretionary decisions to take regarding the set-up of the machine and/or the planning of the measurements. Some attempt to automate this decision making has been investigated by Zhang et al [16]. In this investigation, it appeared reasonable to ascertain whether some of these decisions may have a significant effect on the uncertainty of measurement expressed in terms of  $rmse$ .

The set-up parameters chosen as discretionary factors were the probe extension, the stylus length and the number of probing points. For the probe extension, three different set-ups of the analysed CMM were considered: without any probe extension, with probe extensions of length 100 mm and 200 mm. Three styli of the same type and geometrical characteristics (e.g. material, tip size), but with lengths 20, 60 and 110 mm, respectively, were chosen. Regarding the planning of the measurements, the potential effects on the uncertainty of measurement due to two different numbers of probing points (seven and eleven) were examined.

A kinematic probe with a standard force module was used throughout this experiment. The factors examined in this study with their levels are displayed in Table 2.

FACTORS	LABELS	LEVELS
Room temperature ( °C )	$temp_{(j)}$ $j = 1, \dots, 72$	20      24
Feature	$fea_{(j)}$ $j = 1, \dots, 72$	Ring (R)    Sphere (S)
Probe extension (mm)	$pe_{(j)}$ $j = 1, \dots, 72$	0            100          200
Styli length (mm)	$sl_{(j)}$ $j = 1, \dots, 72$	20           60           110
No. of probing points	$np_{(j)}$ $j = 1, \dots, 72$	7                            11

**Table 2. Experimental factors with labels and levels**

### Randomisation issues

A fully randomized experimental design with three factors at two levels each and two factors at three levels each identifies 72 different experimental conditions, henceforth also referred to as treatments or cells of the design. Three replicates of the design were considered, i.e.  $r = 1, 2, 3$ . This resulted in an overall experimental effort of 216 measurement tasks, i.e. 648 measurement tests.

In the experimental set-up examined, it is not practical to assign randomly a measurement task in a pre-specified experimental condition to the run order, due to the fact that some of the considered factors are hard-to-change. In particular, the air temperature cannot be changed easily. So all the measurement tasks at one level of temperature were carried out first, and then all the others were performed at the remaining level of temperature investigated.

Therefore, if some nuisance factor occurred while performing the measurement task at a certain temperature, it would lead the experimenter to attribute incorrectly such effects on the response variable ( $rmse$ ) to the temperature. Accounting for such possibility, would require the experimenters to replicate all the measurement tasks performed in one day at a certain temperature a number of times (i.e. a number of days) sufficiently large to estimate the variability of the response variable from day to day. This would dramatically increase the experimental burden in a way which is inconsistent with the main objectives of this

investigation. Only one day at each level of temperature was therefore considered. This is the reason why, the reader must exert caution and not to neglect the possibility that the effects attributed to the temperature are in reality due to some lurking nuisance factor. However, in the authors' point of view, the extremely controlled conditions in which the experiment was carried out makes unlikely that such nuisance factors would have indeed occurred. The two types of the features, ring and sphere, were not randomly assigned to the run order. In fact, the sequence of measurement tasks was constructed as a sequence of pairs, each consisting of one measurement of the ring and one of the sphere in identical experimental conditions. This experimental strategy was adopted with the intent of counteracting the potential presence of nuisance factors that increase the variability of the response variable, thus making it more difficult to identify any significant effect on the response variable due to the type of the feature measured.

Once, the room temperature was set and the constraint on the run order for the type of features was introduced, all the others combinations of factors were randomly assigned to the sequence of the measurement tasks.

It is worth mentioning that when changing the probe extension or the stylus length a calibration procedure was run. Consequently, the random assignment of the experimental conditions to the order of the measurement tasks may result some times in a calibration procedure being run, but in some other time in no calibration procedure being run. The last circumstance happens when the probe extension or the stylus length are not changed between two consecutive conditions. This is considered acceptable because this experiment is meant to be representative of the actual operational conditions in which the measuring system is used. In such circumstances, the random sequence of calibration and non-calibration is most likely to happen depending on the variety of measuring tasks performed.

It is moreover argued that performing calibration procedures during the experiment may increase the overall measured uncertainty of the system in comparison with ideal laboratory conditions.

### **Exploratory data analysis**

The  $\hat{rmse}$  is composed of two additive terms of equal importance: an estimate of the variance of a measurement result and an estimate of its bias. Each of the experimental factors considered in this

study may affect differently each of the two components. The effects of the room temperature are graphically examined to demonstrate this observation.

The estimated bias at each temperature for both the ring gauge and sphere is displayed in Figure 3, which as the following figures was obtained in R, a language and environment for statistical computing and graphics [12]. The temperatures displayed on the abscissa do not represent actual values of the temperature at which each measurement result was obtained. They are instead obtained by artificially adding to the original categorical abscissae (21 and 24 °C) an horizontal random component to reduce the occurrence of overlapping points and so to enhance the clarity of the figure ( this technique is called jittering).

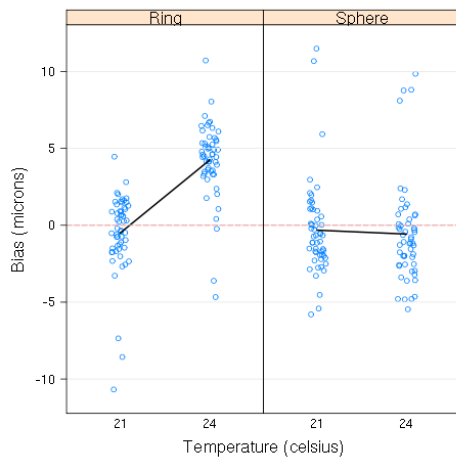


**Figure 3 Effect of the temperature on the bias for the ring and the sphere.**

At the lower level of temperature, the bias distribution for both features is centred close to zero, whereas at the higher level of temperature there is a positive shift of the bias only for the ring. This induces a strong suspicion that there is a significant interaction effect of temperature and feature on the estimated bias. From a practitioner's perspective, this means that uncontrolled variations of air temperature may induce negligible bias on parts with some specific geometric characteristics but a very large bias on others.

On the other hand, this interaction effect may also be attributed to the inadequacy of thermal expansion model expressed in equation 2 when applied to the ring gauge. Further measurement tests involving a ring gauge calibrated at the investigated air temperature would be needed to clarify the matter, but they would be beyond the scope of this investigation.

In Figure 4 the sample standard deviations of the measurement results are displayed. For both the ring and the sphere, no significant effect of the air temperature on the variability of the results is apparent from an examination of this figure. In fact, while considering increased air temperature, only a mild increment in the average standard deviation of the measurement results grouped by temperature is observed in Figure 4.

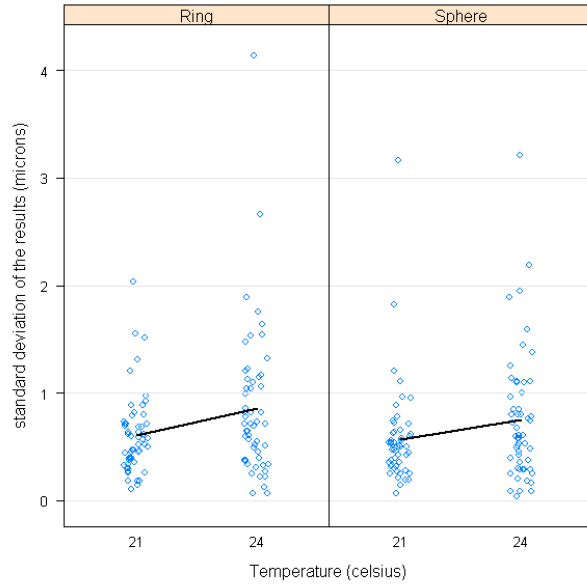


**Figure 4 Effect of the temperature on the sample standard deviation for the ring and the sphere**

Under these circumstances, it is therefore argued that, when increasing the air temperature, the significant increment of  $\hat{rmse}$  displayed in Figure 4 for the ring only can be mainly attributed to the bias. In Figure 4 it can be noticed that the  $\hat{rmse}$ 's are not symmetrically distributed around their average values, when grouped by the temperature. More data points are apparent in the region between zero and the group averages, i.e. the end points of the two continuous segments, than in the region above such group averages. The skewness of the distribution of the  $\hat{rmse}$ 's is independent from the way they are grouped and has implications on the formulation of plausible statistical models for the experimental data. These implications are discussed in the next section.

### Statistical model

A first attempt model that could be considered suitable to describe the experimental results is as follows:

$$\hat{rmse}_j = \mu + temp_{(j)} + fea_{(j)} + pe_{(j)} + sl_{(j)} + np_{(j)} + temp : fea_{(j)} + \dots + er_j \quad (3)$$

In equation (3), the symbol  $\mu$  represents the mean of the response variable  $\hat{rmse}_j$  over all the experiment and  $j = 1, \dots, 72$  is the index associated with each of the experimental conditions. The

meaning of the other symbols is summarised in Table 2, whereas the colon is used to identify an interaction effect on the response variable due to the factors it divides. The parenthesised subscripts map the rows in the data to the levels of the factor used in that row. For example,  $temp_{(j)}$  corresponds to the temperature used for that  $j$ . For brevity, the ellipsis stands for all the remaining possible second order interactions. Interactions of higher order, i.e. involving more than two factors, were not considered because it is difficult to foresee how the experimental conditions considered could possibly cause them. Moreover, from a practitioner's point of view, it is also difficult to see how the awareness of the significance of a third, fourth or fifth order interaction could enrich the knowledge of the measuring system investigated. The terms  $er_j$ 's are random variables that, without losing generality, are assumed to be independent and identically distributed with mean zero and constant variance  $\sigma_{er}^2$ . If they are also normal statistical inferences regarding the parameters of the model is facilitated.

In the previous section it was observed that the realisations of  $\hat{rmse}_j$  are distributed asymmetrically. This circumstance makes it very unlikely that the errors of the model to follow a symmetrical distribution such as the normal. For this reason, it would make the inferential process easier if the response variable were transformed in such a way to assume a more symmetrical distribution. A transformation that appears to suits this purpose is the logarithm. Therefore the following model was considered:

$$\log(\hat{rmse})_j = \mu + temp_{(j)} + fea_{(j)} + pe_{(j)} + sl_{(j)} + np_{(j)} + temp_{(j)} : fea_{(j)} + \dots + er_j \quad (4)$$

Equation (4) represents a multiplicative model in the domain of the untransformed response variable. It can in fact be rewritten as in its equivalent form:

$$\hat{rmse}_j = e^{\mu} \cdot e^{temp_{(j)}} \cdot e^{fea_{(j)}} \cdot e^{pe_{(j)}} \cdot e^{sl_{(j)}} \cdot e^{np_{(j)}} \cdot e^{temp_{(j)}:fea_{(j)}} \cdot e^{temp_{(j)}:pe_{(j)}} \cdot \dots \cdot e^{er_j} \quad (5)$$

This model was fitted to the experimental data using the ordinary least squares method (OLS) as implemented in R [12]. A large number of two-way interactions were found not to be statistically significant resulting in the following final model:

$$\begin{aligned} \log(\hat{rmse})_j = & \mu + temp_{(j)} + fea_{(j)} + pe_{(j)} + sl_{(j)} + np_{(j)} + \\ & + temp_{(j)} : fea_{(j)} + pe_{(j)} : sl_{(j)} + fea_{(j)} : np_{(j)} + er_j \end{aligned} \quad (6)$$

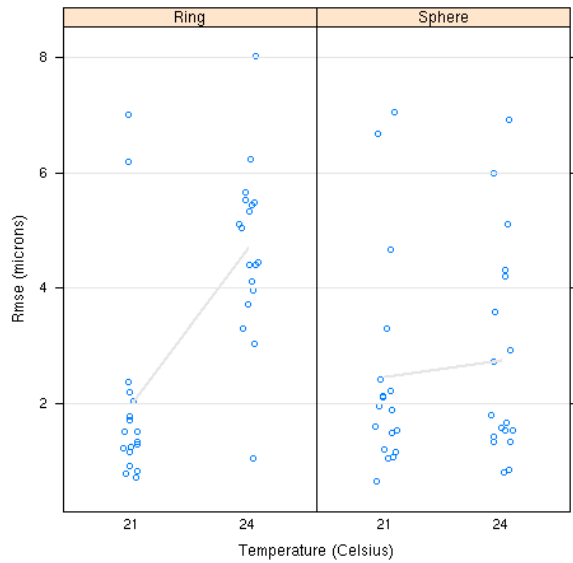
The coefficient of determination ( $R^2$ ), was equal to 40.9 %. This means that about 60% of variability of the response variable is not accounted for by this model and must be due to other unknown sources.

The ANOVA table that shows the significance of each of the factors included in equation (6) is displayed in Table 3.

	Degree s of freedom	Sum of squares	Means of squares	F value	Pr(> F)
Temperature $temp_{( )}$	1	5.78	5.78	30.43	$8.41 \cdot 10^{-7}$
Probe extension $pe_{( )}$	2	4.06	2.03	10.67	$1.13 \cdot 10^{-4}$
Stylus length $sl_{( )}$	2	2.28	1.14	5.99	$4.31 \cdot 10^{-3}$
Type of feature $fea_{( )}$	1	0.879	0.879	4.63	$3.56 \cdot 10^{-2}$
Number of probing points $np_{( )}$	1	0.783	0.783	4.12	$4.70 \cdot 10^{-2}$
$temp_{( )} : fea_{( )}$	1	3.57	3.57	18.8	$5.83 \cdot 10^{-5}$
$pe_{( )} : sl_{( )}$	4	4.52	1.13	5.95	$4.39 \cdot 10^{-4}$
$np_{( )} : fea_{( )}$	1	1.18	1.18	6.22	$1.55 \cdot 10^{-2}$
Residuals	58	11.0	0.190		

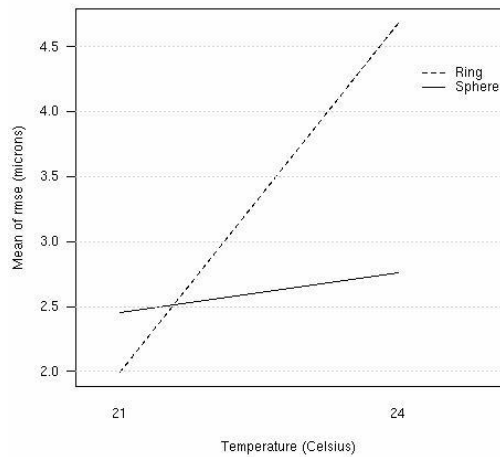
**Table 3. Significance of the factors of the fitted model**

Figure 6, 7 and 8 show interaction plots corresponding to the three significant interaction effects in the final model. These show the mean  $\hat{m}se$  for each combination of the interacting factors and are useful in interpreting the combined effect of these factors.



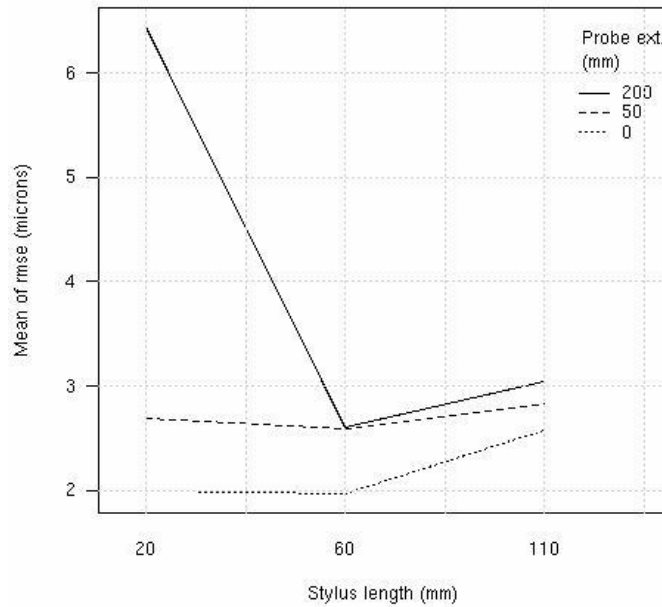
**Figure 5** Effect of the temperature on the  $\hat{rmse}$  for the ring and the sphere

The significance of the interaction between temperature and type of feature that was expected by the observation of Figure 5 is confirmed by Figure 6 and it has already been discussed in the exploratory data analysis section.



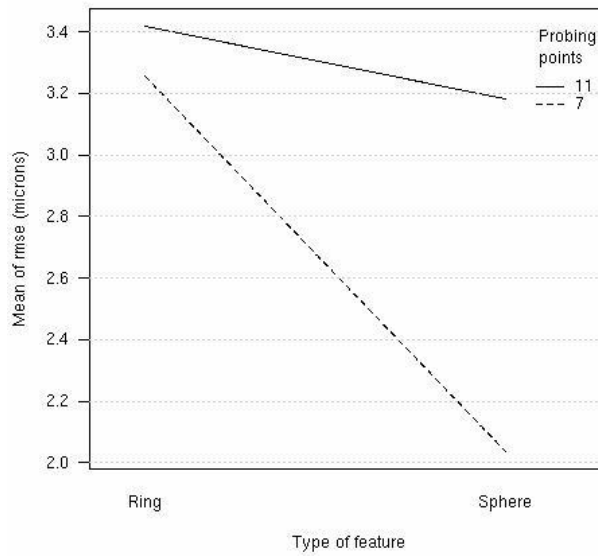
**Figure 6** Interaction effect of the temperature and the type of feature measured (ring and sphere)





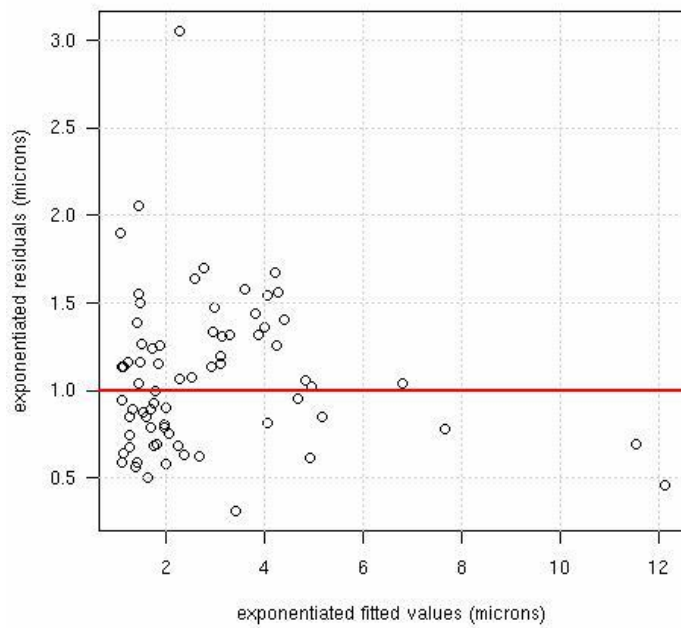
**Figure 7 Interaction effect of the stylus length and the probe extension**

Figure 7 shows that in the selection of the stylus length to obtain improved uncertainty performance, the probe extension must be also considered. For different probe extensions, different styli may be preferable from the point of view of limiting the uncertainty. Stylus length and probe extension should therefore be chosen together. In Figure 7, this is demonstrated observing that with the same probe extension of length 200 mm, uncertainty of measurement can be greatly improved if the stylus length is carefully chosen (stylus length 60 mm). Moreover, the same figure suggests that a set-up that does not make use of any probe extension can produce measurement results with improved uncertainty, independently from any specific stylus length. It also appears that the stylus with length 60 mm has superior uncertainty performances in absolute terms and also in terms of robustness to changes of probe extension.



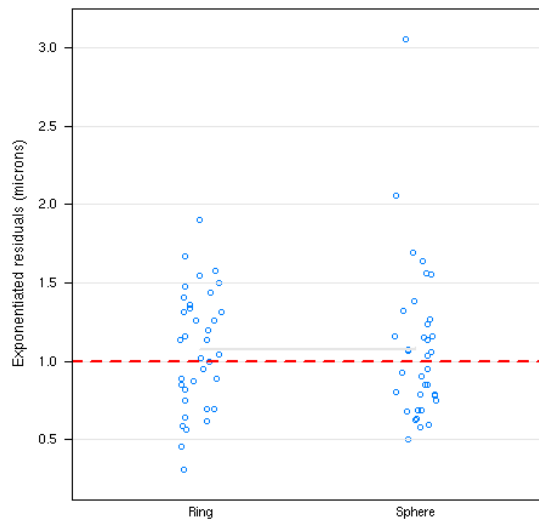
**Figure 8 Interaction effect of the type of feature and the number of probing points**

Figure 8 supports the intuitive idea that in the selection of the number of probing points the type of feature to be measured has a part in affecting the uncertainty of measurement that will be achieved. The same number of probing points that provides satisfactory uncertainty on a specific feature may lead to deteriorated uncertainty performances when different type of features are measured.



**Figure 9 Exponentiated residuals versus exponentiated fitted values**

The assumptions underlying the model of equation 6 are graphically tested by examining the residuals. Figure 9 shows the exponentiated residuals against the exponentiated fitted values. Both the residuals and the fitted values have been exponentiated to convert them back to the micron scale. This also means that the residuals must be interpreted multiplicatively (equation 5). Hence, a value of one indicates a perfect fit to the model whereas the few larger residuals indicate observed errors about 5 or 6 times larger than expected. Most importantly, we see no association with the fitted values.



**Figure 10 Realised residuals grouped by type of feature.**

In Figure 10 the realisations of the exponentiated residuals are grouped by type of feature. If the assumptions of independence and identical distribution of the errors is satisfied, the exponentiated residuals should not exhibit any pattern or difference in behaviour however they are grouped. The fact that no differences are apparent in Figure 10 supports the conjecture that all the effects caused by the type of feature on the response variable are correctly captured by the considered model. Therefore, the type of feature does not appear to have any effect on the realisations of the exponentiated residuals.

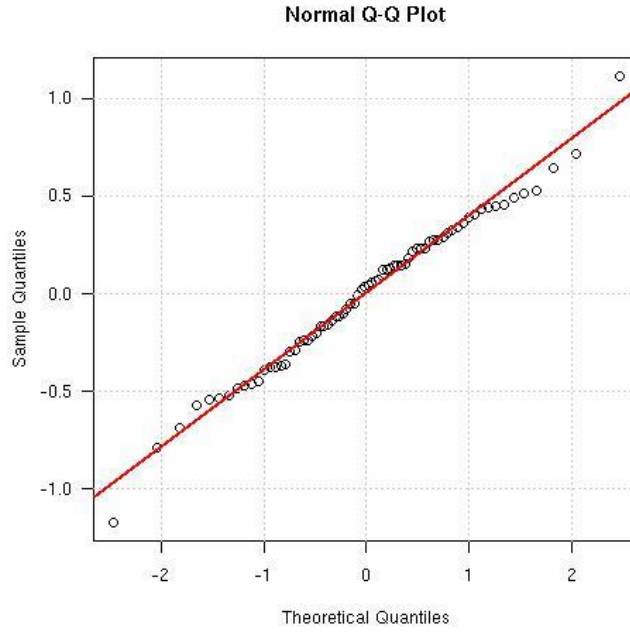


**Figure 11** Quantile-Quantile normality plot of the realised residuals

Figure 11 shows a Q-Q plot to assess the normality of the errors, which seems to be confirmed.

One final concern is the lack of a full randomisation in our experimental design due to practical considerations. In particular, for each setting of the experimental factors, we perform the ring and sphere measurements together. We can modify our model to take account of this as follows:

$$\begin{aligned} \log(\hat{rmse})_j = & \mu + temp_{(j)} + fea_{(j)} + pe_{(j)} + sl_{(j)} + np_{(j)} + \\ & + temp_{(j)} : fea_{(j)} + pe_{(j)} : sl_{(j)} + fea_{(j)} : np_{(j)} + pa_{(j)} + er_j \end{aligned} \quad (7)$$

The term  $pa_{(j)}$  is a random effect with mean zero and some variance to be estimated. There will be one such term for each pair of a ring and sphere measurements, i.e. 36 pairs in total. Such a model is called a mixed effects model and is described in [14]. The hypothesis that the variance of  $pa_{(j)}$  is zero can be tested using a parametric bootstrap method as long as we assume normality of the random effect. In this case, the term is found not be statistically significant (p-value=0.46). Thus, it is reasonable to conclude that there is no association between these pairs of measurements and that the lack of a full randomisation has had no consequence. Nevertheless, it is wise for experimenters to investigate these concerns in similar designs where practicality precludes a full randomization.

## Conclusions

Often in industrial environments the adequacy of the measurement system to perform a measurement task may be assessed solely on the basis of random error evaluations. Repeatability studies can be considered among this kind of approaches. The state of calibration of the measurement system should instead provide assurance of the lack of systematic error (bias) when performing a measurement task in the same conditions for which the instrument was calibrated. *rmse* was analysed as a single parameter that provides the practitioner with a tool to monitor the performance of the measurement system in terms of both random and systematic error. The effect of the environment temperature, feature type, probe extension, stylus length and number of probing points on *rmse* were considered by fitting a linear random effect and a linear mixed-effect statistical model to the experimental results. All these five factors were found to be statistically significant. The significance of all the second order interactions of these factors was also considered and only three of them were found to be statically significant (temperature with feature type, probe extension with stylus length and number of probing points with feature type).

The nominal performances of a CMM are evaluated in a pre-specified allowable range of experimental conditions. Even when the machine is meant to be deployed within such a range, the degrees of freedom left to the operators when setting-up the machine or preparing a measurement plan, may lead to significantly deteriorated performances with detrimental effects on the pertinent costs. Among these, there are for example the costs sustained for unnecessary reworking, the costs for the rejection of good parts and costs due to increased failure rate of the final products caused by the acceptance of defective components.

Performances of a CMM should therefore be evaluated in experimental conditions as close as possible, ideally identical, to those in which the machine is meant to be actually deployed. Such experimental conditions should encompass both uncontrollable factors (temperature and parts, in this study) and controllable (settings such as probe extension, stylus length and number of probing points, for example).

## Acknowledgements

The authors gratefully acknowledge Rolls-Royce plc for their financial contribution and the Interdisciplinary Research Centre (IRC) in Materials for High Performance Applications at the University of Birmingham for granting one of authors the use their facilities.

## References

- [1] ISO 10360-1:2001, Geometrical Product Specifications (GPS)-Acceptance and reverification tests for coordinate measuring machines (CMM). International Organisation for Standardisation. 2001.
- [2] ANSI/ASME B89.4.1:1997, Methods for performance evaluation of coordinate measuring machines (CMM).
- [3] VDI/VDE 2617:1989, Accuracy of coordinate measuring machines (CMM), Part 3, components of measurement deviation of the machine.
- [4] International Vocabulary of Basic and General Terms in Metrology (VIM), reproduced verbatim in PD 6461-1:1995. General metrology – Part 1: Basic and general terms (VIM). BSI – British Standards Institution. 1995.
- [5] Guide to the expression of uncertainty in measurement (GUM), reproduced verbatim in PD 6461-3:1995. General metrology – Part 3: Guide to the expression of uncertainty in measurement (GUM). BSI – British Standards Institution. 1995.
- [6] Hermann, G. Geometric Error Correction in Coordinate Measurement. *Acta Polytechnica Hungarica*, 2007, 4(N1), 47-61.
- [7] Feng, C-X J. Pandey, V. Experimental study of the effect of digitising parameters on digitising uncertainty with a CMM. *International Journal of Production Research*, 2002, 40(N3), 683-697.
- [8] Feng, C-X J. Saal, A. Salsbury, J. Ness, A. Lin, G. Design and analysis of experiments in CMM measurement uncertainty study. *Journal of Precision Engineering*, 2007, 31(N2), 94-101.

- [9] Miguel, P. King, T. Abackerli, A. CMM touch trigger performance verification using a probe test apparatus. *Journal of the Brazilian Society of Mechanical Sciences and Engineering*, 2003, 25(N2), 1-16
- [10] Mood, A. Graybill, F, Boes, D. Introduction to the theory of statistics. 3<sup>rd</sup> edition, McGraw-Hill, 1974
- [11] ISO/TS 15530-3:2004 Geometrical Product Specifications (GPS) – Coordinate measuring machines (CMM): technique for determining the uncertainty of measurement – Part 3: Use of calibrated workpieces or standards. International Organisation for Standardisation. 2004.
- [12] R Development Core Team. A Language and environment for statistical computing. R Foundation for Statistical Computing, Vienna, Austria. ISBN: 3-900051-07-0. URL: [www.r-project.org](http://www.r-project.org) . 2008.
- [13] Hirotsugu, A. A new look at the statistical model identification. *IEEE Transactions on Automatic Control*. 19(N6), 716-723.
- [14] Jose' C. Pinheiro and Douglas M. Bates. Mixed-Effects Models in S and S-plus. Springer. 2000.
- [15] Collins, C E. Fay, E B. Aguirre-Cruz, J A. Raman, S. Alternate methods for sampling in coordinate metrology. *Proc. IMechE*

## Appendix

### Notation

$temp_{( )}$  Room temperature ( $^{\circ}\text{C}$ ).

$\alpha_{T_{ref}}$  Coefficient of linear thermal expansion at  $T_{ref}$  .

$fea_{( )}$  Feature measured, i.e. ring or sphere.

$pe_{( )}$  Probe extension (mm),.

$sl_{( )}$	Styli length (mm).
$np_{( )}$	Number of probing points.
$\theta$	Value of a measurand alias true value of a measurand.
$\hat{\theta}$	Estimate of the value of a measurand with the certified reference material at $T_{ref}$ .
$\mu$	Overall mean or intercept in a linear statistical model.
$\hat{\theta}_T$	Estimate of the value of a measurand with the certified reference material at $T$ .
$\hat{\sigma}$	Estimate of the standard deviation of a single test.
$\sigma_{er}^2$	Variance of the errors of a statistical model.
$e$	Error of measurement.
$e_r$	Random error.
$e_s$	Systematic error.
$er_x$	Random errors in a statistical model indexed by the series of subscripts $x$ .
$rmse$	Root mean squared error.
$\hat{rmse}$	Root mean squared error.
$S^2$	Sample variance of a series of tests.
$T$	Generic temperature.
$T_{ref}$	Reference temperature stated in the calibration certificate.
$\bar{x}_i$	i-th measurement result in a series of $n$ measurements.
$\bar{x}$	Generic measurement result of a measurement task calculated as average of a series of measurement tests.
$\bar{x}$	Average of large number of generic measurements ( $\bar{x}$ ).
$\bar{x}_\infty$	Average of an infinite number of generic measurements ( $\bar{x}$ ).





## Appendix 3 – Pundit/CMM Evaluation (Extracted from Rolls-Royce 1<sup>st</sup> year Engineering Doctorate technical report)

### Introduction

Manufacturers need to use complex measuring instruments such as coordinate measurement machines (CMMs) and other measurement devices to verify that parts are properly made, but use of these instruments can be time-consuming and expensive. Manufacturers need a method to develop and test measurement strategies before manufactured components enter the factory floor. NIST has been developing mathematical algorithms to help manufacturers optimize the use of their measurement instruments. Recently NIST developed computer simulation methods used to estimate the accuracy of measurements in manufacturing applications. MetroSage used NIST research to develop their "PUNDIT/CMM" software system that allows computer simulation of factory measurements without requiring a slowing or stoppage of the production line. The software became commercially available in January 2004. [6] Several U.S. manufacturers, including Ford, Boeing, and Caterpillar, have pre-purchased PUNDIT/CMM software to assist in their manufacturing measurements. The U.S. Air Force and the Department of Energy have acquired PUNDIT/CMM for defence related measurements.

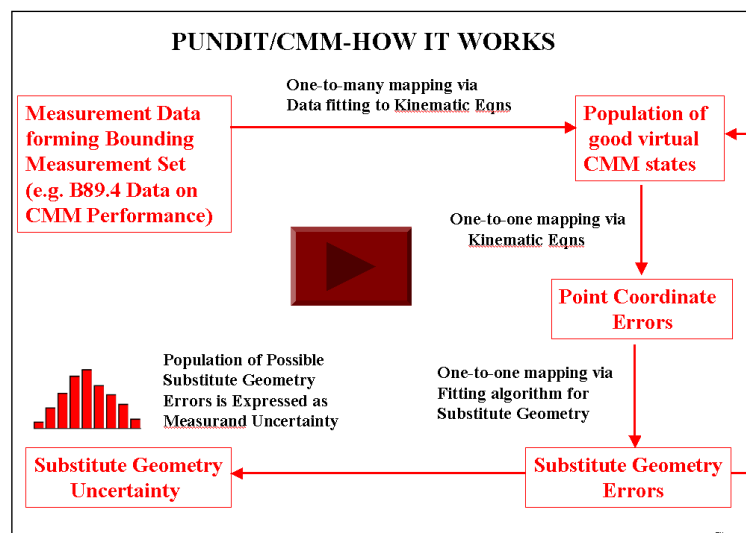


Figure 1. Pundit/CMM structure

## Methodology

The evaluation of the software followed the guidelines of the ISO 15530-4 currently in development.

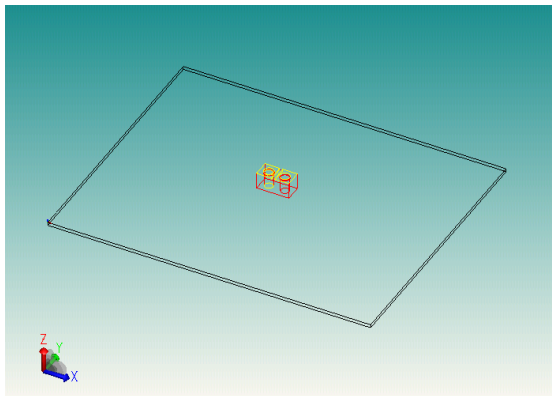
### Reference values

#### a) No Variance Case

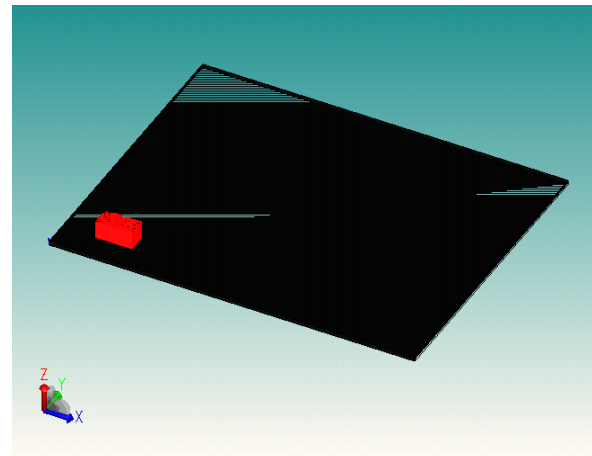
To evaluate such case the only errors selected for the simulations were Probe errors. The CMM selection was perfect, the thermal effects were switched off, the sampling strategy was constant and the form errors were also off.

The part was then placed in the centre volume of the CMM and the uncertainty result was found to be  $1.3 \mu\text{m}$ . Figure 2 shows the placement of the part in the different CMM volumes.

a)



b)



c)

d)

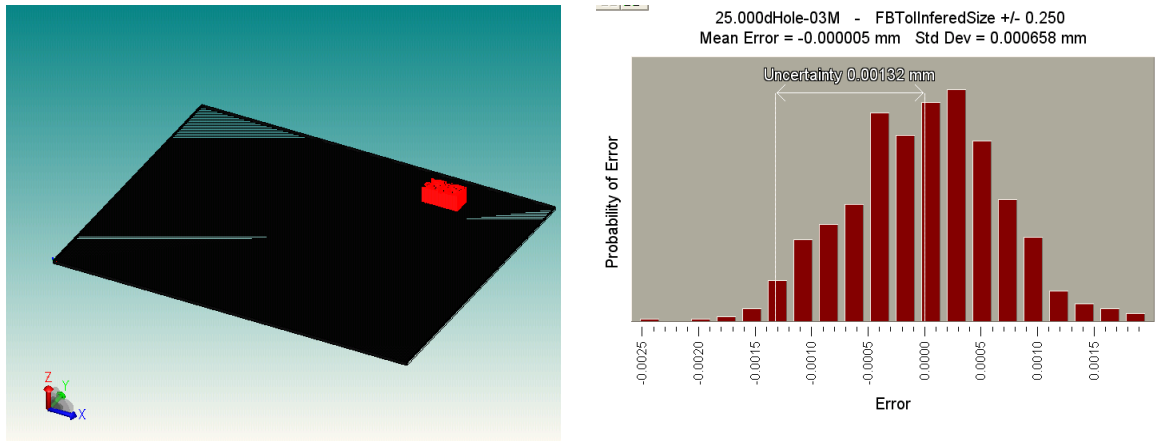


**Figure 2. a)b) and c) Part placement in the CMM volume. d) Measurement uncertainty of a,b,c.**

The uncertainty value for the different placements was found to be always the same 1.3  $\mu\text{m}$ .

b) Zero case

The zero uncertainty case is a case in which the sources of error are set to zero and therefore the results should be 0. This case was found to be true.

c) Thermal effect case

This case is based on the components thermal expansion coefficient. The change in length:

$$\Delta L = L_0(\alpha)(\Delta T) \quad (4)$$

Where  $L_0$  is the original length,  $\alpha$  is the thermal expansion coefficient and  $\Delta T$  is the change in temperature.

To simulate this situation in Pundit the CMM was set to perfect machine, the probe model to perfect fixed single tip and the thermal expansion coefficient to 10 ppm/ $^{\circ}\text{C}$  and the work

piece temperature to 50 °C. The measured length, 100mm was the width of the part shown in figure 3. With the standard temperature of the work piece set to 20 °C the change in length:

$$\Delta L = 100(10^{-5})(50 - 20) = 0.03mm \quad (5)$$

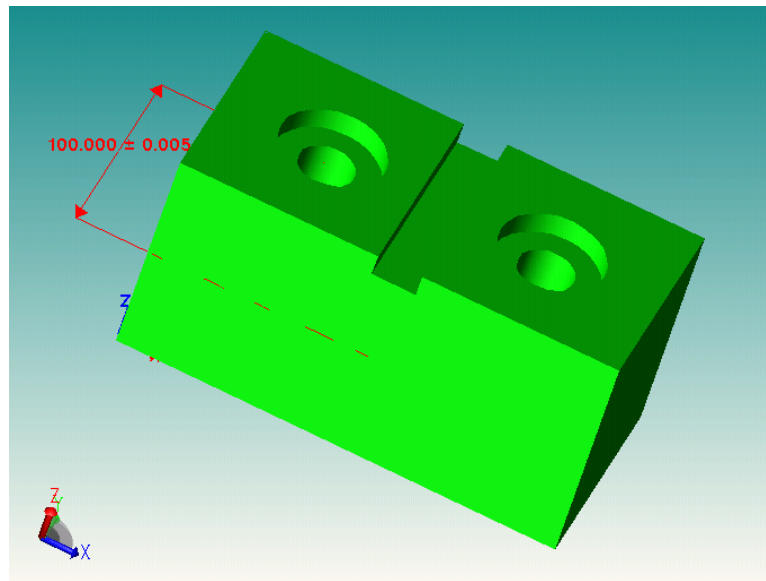


**Figure 3. Part width to be measured**

In this case the calculated uncertainty should have a systematic error of 30 μm and it did so.

### Physical measurement

The physical measurement experiment consisted of the following steps:

- 1- Define the machine coordinate system and ring gauge coordinate as being the same.
- 2- Define three point sampling strategy in the ring gauge. The points are equidistant at an angle theta.

3- Rotate the machine coordinate system with respect to the gauge coordinate system in steps of  $10^\circ$  36 times.

4- Evaluate the standard deviation for the radius of the gauge.

5- Change the angle theta between the 3 points in steps of  $10^\circ$ . Repeat steps 1 to 4.

The values obtained will then be compared to the values in section d).

#### d) Analytical comparison

Some specific uncertainty results can be determined analytically. S. D. Philips et al gave an example of such method for the case of small circular features. Their work examined the measurement uncertainty of small circular features as a function of the sampling strategy. A three-point sampling strategy (figure 4), in which the angle between each point varied from  $1^\circ$  to  $120^\circ$ . was used.

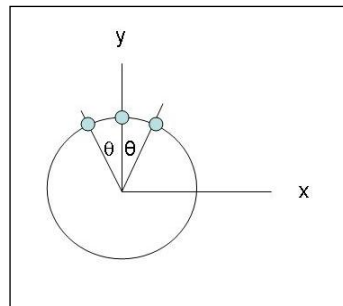


**Figure 4. Three equidistant points sampling strategy**

Equations (6) (7) and (8) used by [7] were derived from first principles [NISTIR 5501] to evaluate the sensitivity of three-point circle fitting parameters. Such equations were based on the equation of a circle passing through three points  $(x_i, y_i)$  for  $i = 1,2,3$ .

$$x^2 + y^2 + ax + by + c = 0 \quad (6)$$

The center of the circle was identified by:

$$(-a/2, -b/2) \quad (7)$$

and the radius by:

$$r = \frac{1}{2}(a^2 + b^2 - 4c)^{\frac{1}{2}} \quad (8)$$

A linear system of equations containing each point definition was then written in matrix form to evaluate the coefficients a, b and c. By evaluating the coefficient a, the x component in equation 6 can be found. The standard deviations for the x, y and r components were found to be respectively:

X center:

$$\sigma^2 = \frac{1}{2\sin^2 \theta} \sigma^2 B89 \quad (9)$$

Y center:

$$\sigma^2 = \frac{3}{2(1-\cos \theta)^2} \sigma^2 B89 \quad (10)$$

Radius:

$$\sigma^2 = \frac{1+2\cos^2 \theta}{2(1-\cos \theta)^2} \sigma^2 B89 \quad (11)$$

A 20 mm ring gauge was used for this experiment and its measurement uncertainty estimated via repeated measurements. The factors that influenced the measurement system were kept to a minimum according to the author. Table 1 contains the data for the probes performance test according to the B89 test.

**Table 1. B89 test data**

Probe	$\sigma$ (standard deviation (B89))	
Mechanical (TP 6) 30 mm Stylus	1.14 $\mu\text{m}$	

Although two models were suggested by [3], only one model was recreated in Pundit, the single-parameter model for the radius component.

Having generated the ring gauge model in Pundit the simulation was set according to table 2.

**Table 2. Pundit simulation settings**

Tab	CMM	PROBE	Environment	Measurement Plan	Manufacturing Info
Settings	Perfect Machine	Single tip fixed, Piezoelectric (Table 1 data)	Full temperature compensation	Points=360/ $\theta$ (delete all except first 3 points)	Perfect form

Due to some constrains within Pundit some of the angles separating the points could only be approximated. The results below indicate that Pundit is in good agreement with the theoretical results. From the plot below (figure 5) it is clear that both theoretical and pundit values confirm that the sampling strategy has an effect on the measurement uncertainty. The magnitude of the standard deviation between the angles of 30 and 40 doubles, and between the angles of 30 and 120 this factor increases to 14. This situation could reflect the



importance of using arcs has datum planes, or defining diameters in features such as scallops. The number of points fitted to the arc and the angle between such points will provide different values in terms of measurement standard deviation. The standard deviation will therefore increase with the decrement in the angle between the points.

Table 3. Results for partial arc measurements

		Mechanical TP 6 with 30mm stylus											
Mantechmm Values (uncalibrated)	Pundit Values	X-Position			Y-Position			Radius			std		
Analytical values	Perturbation magnitude	Angle	Uncertainty	std	Uncertainty	std	Uncertainty	std	Uncertainty	std	Uncertainty	std	
1		1	1641.569852	0.046188572	64664188.09	9.167201	64651058	9.16627					
2		2	410.517501	0.023097804	4042127.368	2.291975	4038845.2	2.291044					
Probe Performance (Std B89)		3	9.553661305	0.003523626	798647.6281	1.018785	797189.27	1.017854					
		4	7.167793513	0.003052092	252786.928	0.573168	251966.89	0.572238					
1.2996E-06		5	5.736856623	0.002730496	103588.8523	0.366912	103064.27	0.365981					
		6	4.783386117	0.002493289	49983.95456	0.254871	49619.865	0.253941					
		7	4.102754524	0.002309099	26997.91046	0.187314	26730.593	0.186384					
		8	3.592648267	0.002160786	15837.73944	0.143467	15633.23	0.142538				0.08	
		9	3.196226611	0.002038091	9895.963257	0.113405	9734.5156	0.112477					
		10	2.879385242	0.001934438	6499.010437	0.091903	6368.3643	0.090974				0.054	
		20	1.4619022	0.001378364	412.4300945	0.023152	380.26666	0.02223				0.013	
		30	1	0.00114	83.56921938	0.010421	69.641016	0.009513				0.0055	
		40	0.777861913	0.00100544	27.40466699	0.005968	19.856035	0.00508				0.003	
		50	0.652703645	0.000921007	11.75542216	0.003909	7.1565122	0.00305				0.002	
		60	0.577350269	0.000866213	6	0.002792	3	0.001975				0.0012	
		70	0.532088886	0.000831566	3.4647034	0.002122	1.4250967	0.001361				0.0008	
		80	0.507713306	0.000812296	2.196652104	0.00169	0.7763755	0.001004					
		90	0.5	0.000806102	1.5	0.001396	0.5	0.000806				0.0006	

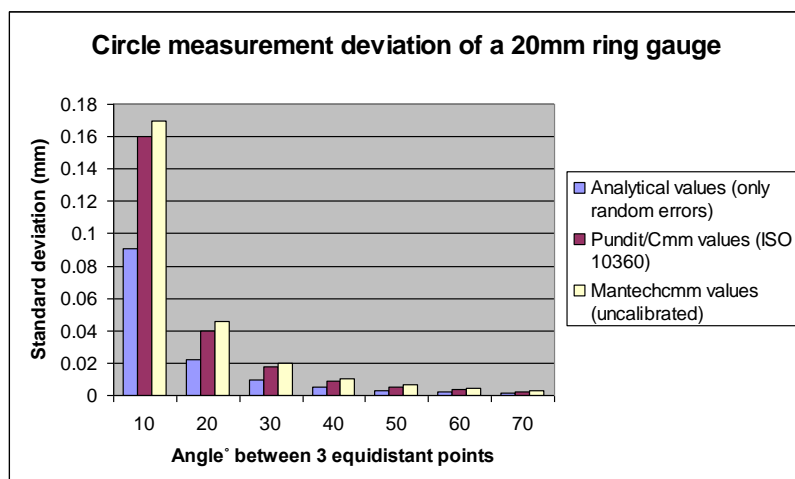


Figure 5. Comparison output results

The physical measurement of the artefact was carried out on an Mitutoyo Apex 776.

## Conclusions

The use of Pundit/CMM as a tool for estimating task specific measurement uncertainty was tested and applied to a “real world” problem. From the literature review presented in section 2.1 it was clear that measurement uncertainty for CMM’s is dependent on many factors. Pundit/CMM was evaluated according to the ISO 15530-4 and the results conformed to the cases used to test the software. The physical evaluation of the software indicated that both the values and trend of the results obtained were in accordance with the work done by [3] and the Apex CMM situated at the HPMC facility. More testing is currently planned for the 1st quarter of 2008 where DOE will be used to finish the software evaluation.

## References

- [1] ISO/IEC Guide 98:1995 Guide to the expression of uncertainty in measurement (GUM), Geneva, 1995.
- [2] N.A. Barakat, A.D. Spence, M.A. Elbestawi, Adaptive compensation of quasi-static errors for an intrinsic machine, *International Journal of Machine Tools & Manufacture* 40 (2000) 2267–2291
- [3] S.D. Phillips, B. Borchardt, W.T. Estler, John Buttress, The estimation of measurement uncertainty of small circular features measured by coordinate measuring machines, *Precision Engineering* 22 (1998) 87-97
- [4] Chang-Xue Jack Feng, A. L. Saal, J. G. Salsbury, A. R. Ness, G. C. S. Lin, Design and analysis of experiments in CMM measurement uncertainty study, *Precision Engineering* (2006)
- [5] K. D. Summerhays, J. M. Baldwin, R. P. Henke, M. P. Henke, The validation of CMM task specific Measurement Uncertainty Software, *Proceedings of the ASPE* (2003)
- [6] [http://www.nist.gov/director/states/ca/fy04\\_ca\\_16.htm](http://www.nist.gov/director/states/ca/fy04_ca_16.htm)
- [7] T. H. Hopp, The sensitivity of three-point circle fitting, *NISTIR 5501* (1994)

## Appendix 4 – Automated Leading edge assessment

### 1. Software specification

#### 1.1 User interface

1.a) Administrator box for two types of user. User ID and Password required for software.

Programmer - Access to all software parameters

Operator - No access to parameters menu. Grey the parameters button, shift button and rotation button.

1.b) Library of acceptance/rejection criteria to be removed from the main screen. A drop down menu should be created for the library. Within the library drop menu 3 options should be available – LESA1. When one of the options is clicked the current library window should then pop-up with a minimize/maximize/close button. See figure 1 below.

1.c) Create a zoom in box by dragging the left mouse button. Create button below the trailing edge button in the zoom area.

1.d) Maintain aspect ratio of blades loaded.

1.e) Window needs to be scaleable and sizable to any screen aspect ratio (eg. Widescreen).

1.f) Library to have the capability of learning new shapes without deleting other predefine shapes.

1.g) Add MSA button to specification. Same format as LESA1.

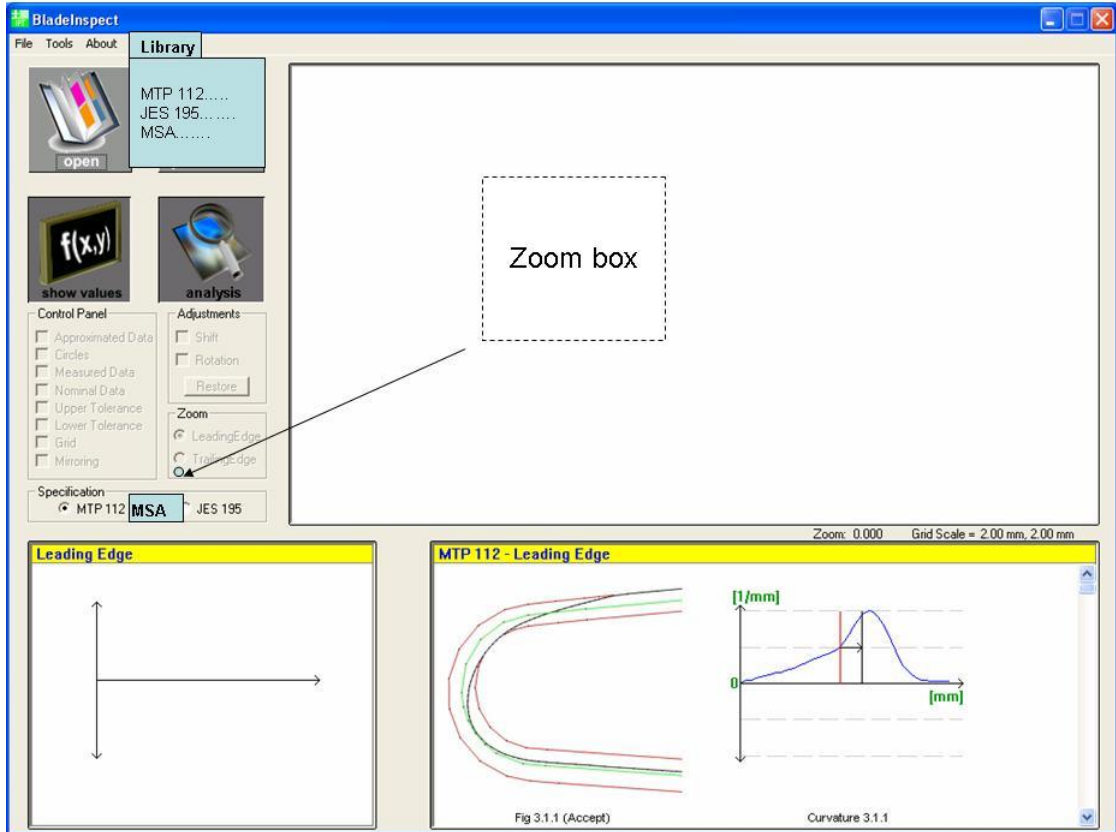


Figure 1. User interface

## 1.2 Data preparation

2.a) Test data points for overlapping and remove overlapping points. This should be available as an option so that the effect of having it on/off can be explored.

2.b) Approximated data to be viewed both as solid line and point distribution. Add new check box in control panel for inclusion of point data in plot.

2.c) Blade Inspect to read .CSV, .GWS, .DXF, .IGES files. (Identify z coordinate)

2.d) The library plots should be updated if the parameters of the analysis change. This will allow for a dynamic library. Add new/ clarify parameters for library.

2.e) Option to import data as single blade or batch process for multiple heights of a blade. Some files will contain several airfoil data for different heights of the same blade such as IGES format where the airfoil can be rebuilt by putting together all the Z heights of the blade.

- When the open menu pops up the user should be able to select an IGES file and type in the heights of interest (figure 2).

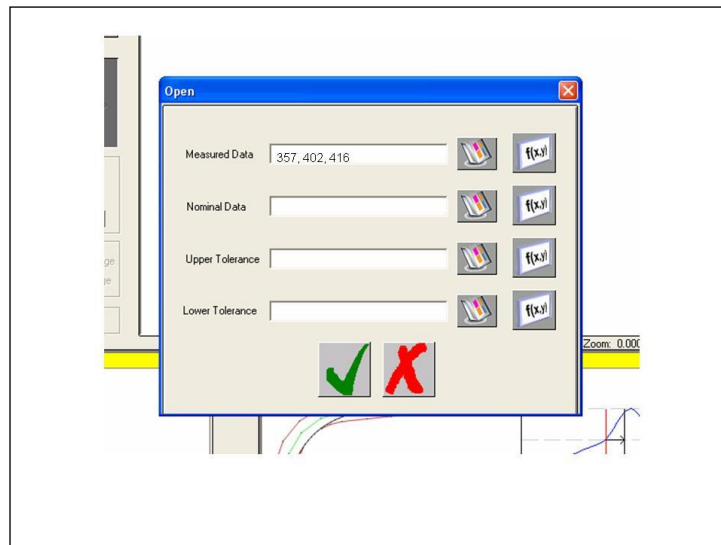


**Figure 2. Open menu with heights of a blade selected for processing.**

2.f) Blade Inspect to automatically capture and process data. (to be defined at a later stage. Possible integration with CMM software or stand alone package that is called from the CMM software)

## 1.3 Parameters

### 3.a) Camber Line definition at the Leading edge

The camber line will be defined by the finding the intersection point of two lines with the following characteristics:

Both variables A and B will be available in the parameters menu as input boxes. This will allow evaluating the effect of the **number of points** and **zone of the leading edge for the line fit** on the camber line definition.

### 3.b) Start and End points for the curvature analysis.

The start and end point of the curvature analysis will be defined as a distance in mm along the camber line. A new box should be added to the parameters menu where the user can change this distance. The distance is highlighted in figure 4 as variable D.

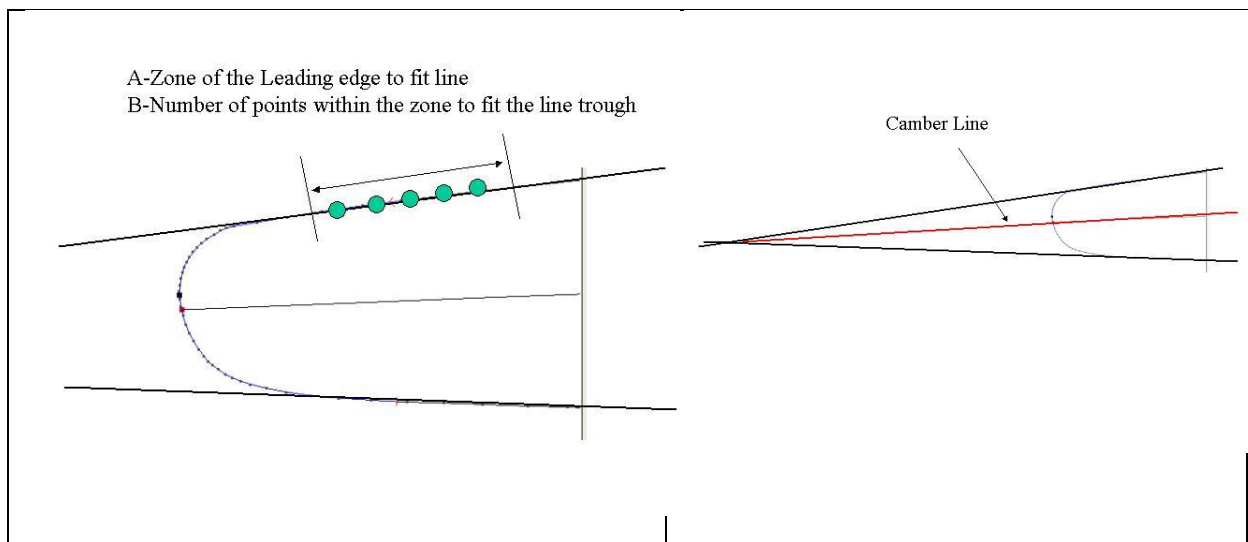


**Figure 3. Camber line definition**



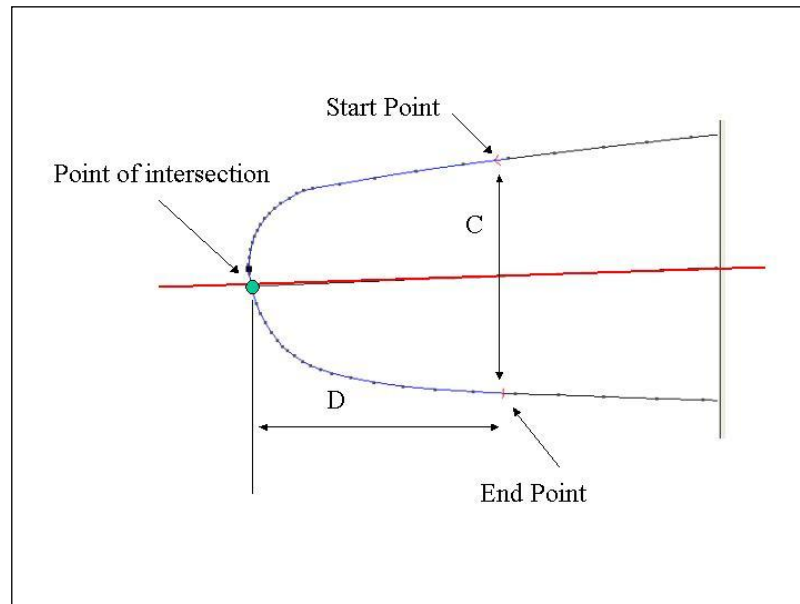


**Figure 4. Start and End points of curvature analysis.**

### 3.c) Curvature plots

3 types of curvature plot will be required:

- 1- Raw data (non dimensional).
- 2- Curvature divided by distance C (figure 5).
- 3- Curvature divided by distance D (figure 5).

The 3 plots should be visible where the library screen is currently placed.

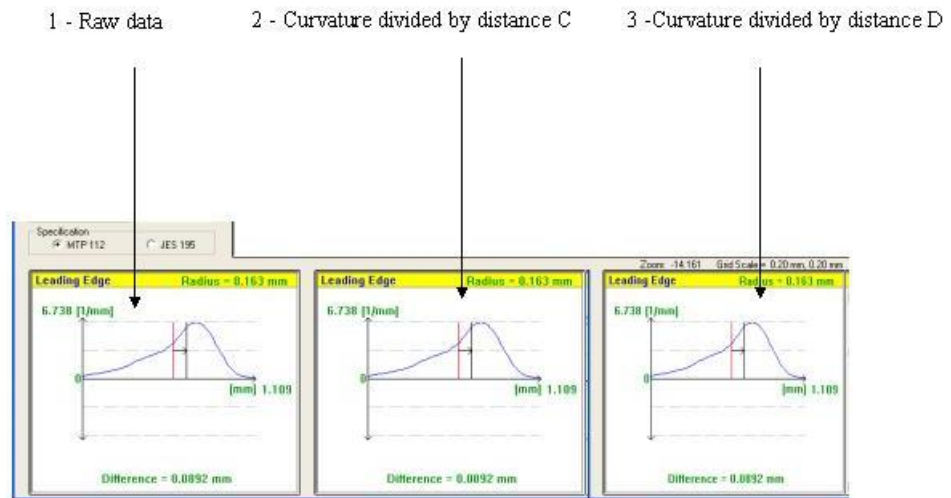


**Figure 5. Curvature plots display in the main screen.**

3.d) Curvature plots outputs

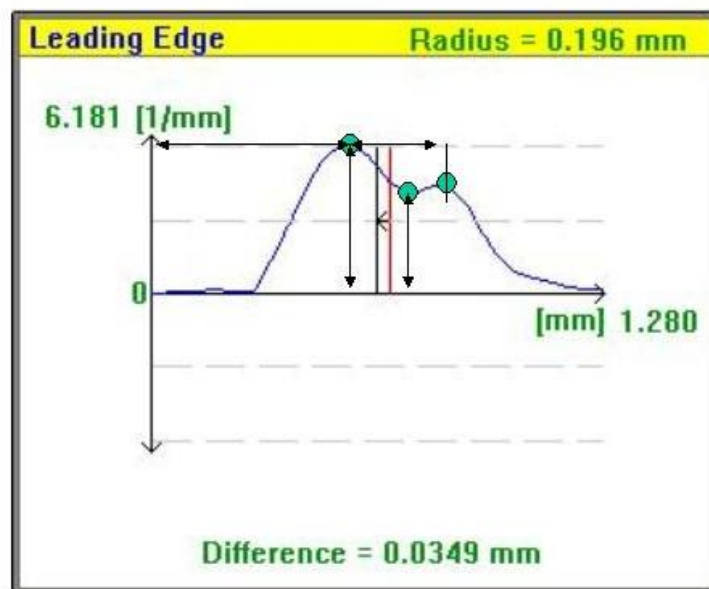


**Figure 6. Curvature plots outputs.**

Every curvature plot should output the x and y coordinate (both nominal and measured data) of the peaks in a txt file together with the following variables:

- 1- Height of maximum peak – indicates excessively sharp blade
- 2- Depth of minimum trough – indicates a flat or hollow
- 3- Distance between two peaks if present (along distance axis)– indicates length of flat
- 4- Peak to trough height (on curvature axis) – indicates excessive change of curvature
- 5- Asymmetry of either a single peak or between double peaks – indicates edge offset.

### 3.e) Spline direction

The spline should always start on the pressure side of the leading edge and progress towards the suction side. Blade inspect will have to interpret airfoil sections with different orientations.

### 3.f) Curvature plot display

Curvature plots to display both nominal and measured data. The number of points used for curvature averaging should be displayed at the bottom right hand corner of the plot screen next to the “difference” statement.

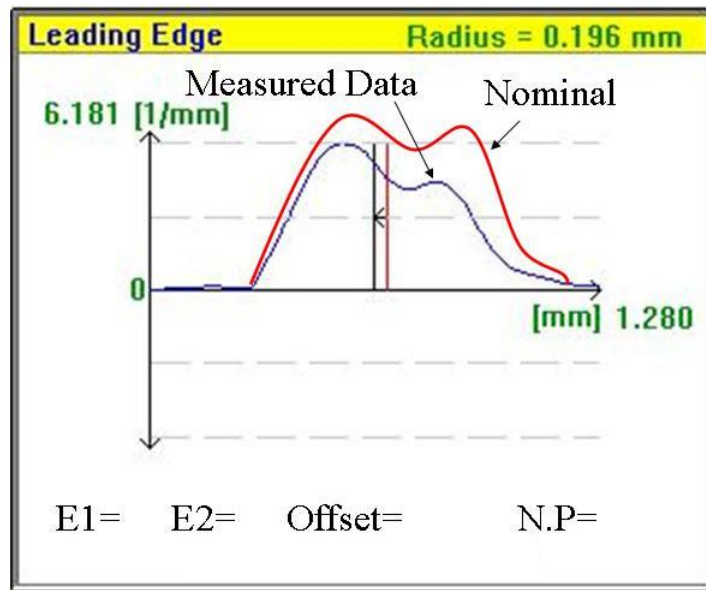


**Figure 7. Curvature plot displaying both the measured data and the nominal data.**

3.g) Weighting factors weights to be unlocked and included in the configuration files.

3.h) Ellipse ratios.

Two ellipses are to be fitted to points 2-3 and points 2-4. Both ratios are to be displayed in the curvature plot as E1=... and E2=...Lengths e and f will be used to calculate an offset which will be the ratio of the two variables. The result will also be displayed in the curvature plot as Offset=...(figure 7).

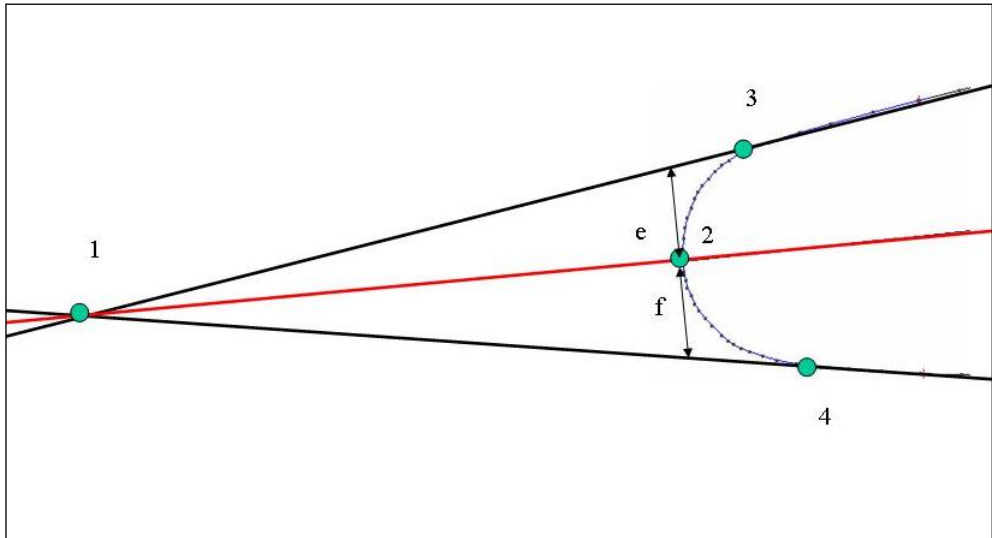


**Figure 8. Ellipse ratio.**

Point 2 is the apex point, the point furthest away along the high curvature area of the leading edge. Point 3 and 4 are the last data points used to fit a straight line along the airfoil. Point 1 is where both lines intersect. A line intersecting both points 1 and 2 is to be created.

### 1.4 Configuration files

4.a) Configuration files to be created in XML. Each configuration file will be blade specific and will contain all the options relating to that blade predefined. The file will include parameters settings, heights to processed, etc. Two example files could be TXXHP, TXXLP.

4.b) Weights and Parameters to be saved on configuration file only during programmer mode. Use the save button in the parameters window to save changes to a configuration file.

### 1.5 Bugs

1- Error boxes in German.

- 2- Error boxes come up when numbers are erased on parameters boxes.
- 3- Default button does not work if one of the parameters box does not contain numbers.
8. Provide Full Documentation

## **2. Mathematical modelling of the leading edge and software testing**

### **2.1 Introduction**

Current business opportunities have indicated that there is space for improvement in some areas where the inspection of airfoil sections takes place, specifically leading edge and trailing edge profiles. The task of passing or failing a profile is currently dependent on the inspector/operator who judges the captured profile against the profile specification. In any process the operator can cause the highest variance and therefore there is a need of automating such process together with a more scientific approach to the current activity.

In this context a software tool is being developed at the Aachen University (aka Fraunhofer Institute, aka IPT, aka WZL), which can take measured blade's coordinate data in a point cloud format and assess it against the appropriate edge profile's spec, i.e. LESA1 for R-R blades. The assessment algorithm is based on curvature analysis based on work done originally by Ian Gower et al., as well as pattern matching techniques. The output is a go/no-go decision that is entirely objective, with no visual assessment needed by the operator or inspector.

In order to prove the capabilities of the tool, a group of tests were and will be carried out. At this document the mathematical basis of the software will be evaluated and the results will be shown.

### **2.2 Blade inspect**

The software is, in a simplified description, divided in Pre-Processing, Processing and Classification. The Pre-Processing stage involves all the mathematic algorithms with the aim of preparing the data to the main data process (read data, approximation, curvature calculation). The Processing stage involves all the algorithms with the aim of extracting the blade characteristics from the curvature graphic. And finally, the Classification stage, which involves the pattern matching algorithm.

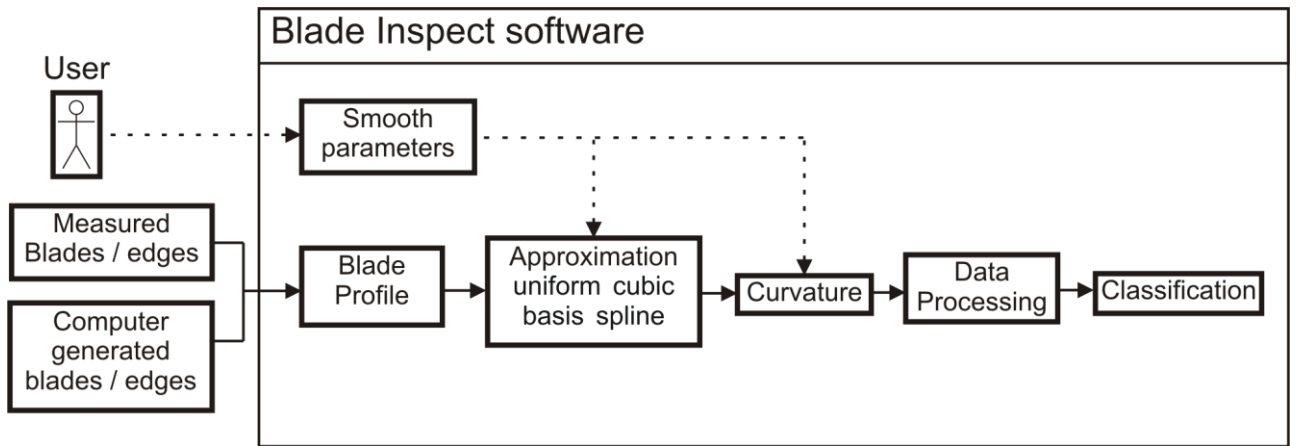


**Figure 1: Software Information flow**

In the next sections the pre-processing steps will be explained and evaluated.

### 2.3 Pre-Processing

The whole assessment chain starts with the measurement method and process, which determines the format in which the information will be recorded. Based on this format the mathematical functions will be chosen and developed.

In this case the format defined is a point cloud, which contains the coordinate positions of the measured blade. These points will describe a transverse slice of this aerofoil, as show in the Figure 2 and Figure 3.

One issue in this step, is that the point density is not constant (see Figure 4), due to the measurement method and the many possible edge shapes, which means that the points don't have a constant distance to each other.

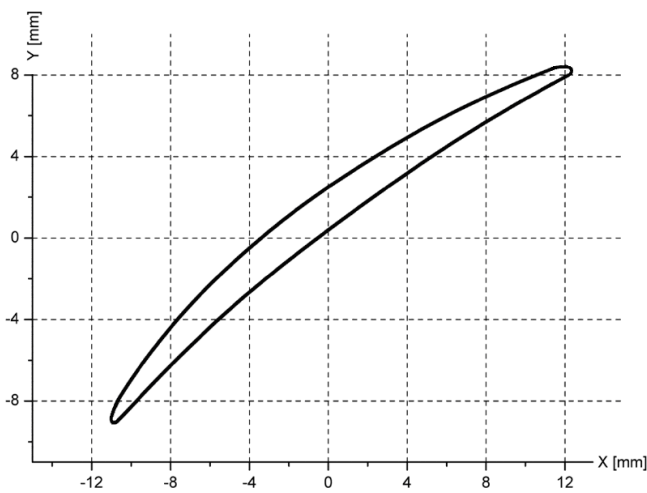


**Figure 2: Measured aerofoil section (transverse view)**

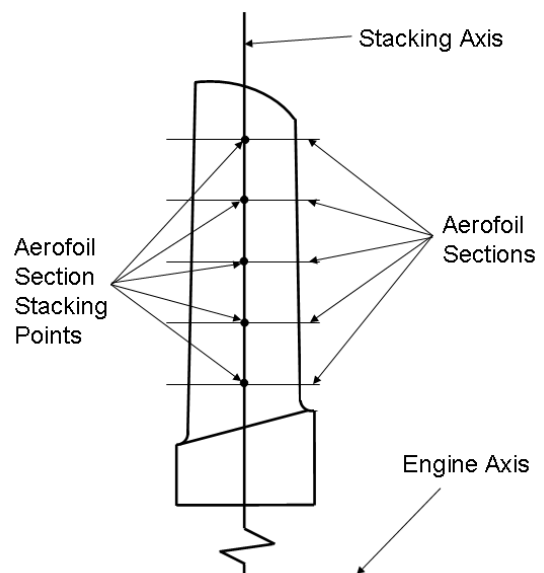


**Figure 3: Aerofoil sections (longitudinal view)**



**Figure 4: measured aerofoil with a not-constant point density**

## 2.4 Curve Modelling Methods

With the purpose of leaving the blade profiles independent from the varying point distance and to guarantee the comparability between different measured blades in the data process and classification steps, a curve modelling method is used. Later on (section 0) a 3<sup>rd</sup> reason for this modelling will be seen.

In the modelling process the notation is the first variable to be set. There is 3 alternative notations, that will be explained below.

- Explicit function:

$$y = f(x), z = g(x)$$

This is the most common notation. But as it is not enclosed related to a rotation (i.e., with a rotation it can occur, that one X-value starts to have 2 Y-values), this kind of function can not be modelled anymore.

- Implicit function:

$$f(x, y, z) = 0$$

This notation is also not able for modelling purposes, as for determined objects a second condition is needed. (for example: a circle can be modelled with  $x^2 + y^2 = 1$ , but if a semi-circle is needed a second condition is required. ( $x > 0$ ))

- Parameterised function:

$$x = x(t), y = y(t), z = z(t)$$

With this notation the issues described before are overcome, because each axis is independent from each other. In this method the curve is approximated piecewise to polynomials, that are normally from the 3<sup>rd</sup> order.



They are normally 3<sup>rd</sup> order polynomials, because polynomials with lower orders are not flexible enough and the ones with higher orders are complex to calculate, as well as have the risk of oscillation. (as it is been shown in the picture below).

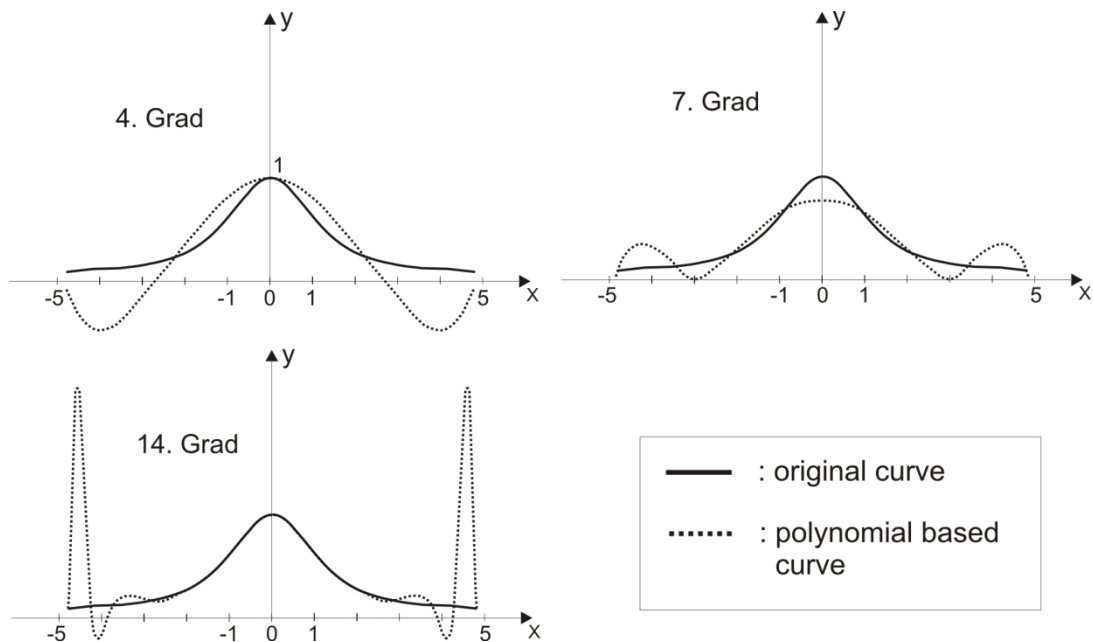


**Figure 5: Example for the oscillation from polynomials from the 4th, 7th and 14th grades.**

Based on the statements described in this section, the notation (Parameterised function) and the polynomial order (3<sup>rd</sup> order) are defined. Parametric cubic polynomials are described using the following equations:

$$Q(t) = \begin{bmatrix} x(t) \\ y(t) \\ z(t) \end{bmatrix} = T \cdot M \cdot G, T = \begin{bmatrix} t^3 \\ t^2 \\ t \\ 1 \end{bmatrix}, G = \begin{bmatrix} P_3 \\ P_2 \\ P_1 \\ P_0 \end{bmatrix} \text{ and } M = \begin{bmatrix} B_{11} & B_{12} & B_{13} & B_{14} \\ B_{21} & B_{22} & B_{23} & B_{24} \\ B_{31} & B_{32} & B_{33} & B_{34} \\ B_{41} & B_{42} & B_{43} & B_{44} \end{bmatrix} \quad \text{Equation 1, 2, 3 and 4}$$

G is the geometry matrix, which is composed of the geometric constraints (points or tangents), and M is a 4x4 Basis matrix. G and M are dependent from the modelling method. The vector Q(t) is made up of 3 cubic polynomials related to the parameter t.

### Geometric and Parametric Continuity

For evaluating the continuity from modelled curves, it is usual to use 2 types of parameters, which describe this characteristic of the model. This parameters are divided in geometric and parametric.

#### Geometric Continuity:

- G0: curves are joined, touch at the join point. words, the curves share a common centre of curvature at the joint point.
- G2: first and second derivatives are proportional at join point. In other words, the curves share a common centre of curvature at the joint point.
- G1: first derivatives are proportional at the join point. [ The curve tangents thus have the same direction, but not

necessarily the same magnitude. i.e.,  $C1'(1) = (a,b,c)$  and  $C2'(0) = (k*a, k*b, k*c)$ . ]. In other words, the curves share

a common tangent direction at the join point.

Parametric Continuity:

- C0: curves are joined.
- C2: first and second derivatives are equal. [If  $t$  is taken to be time, this

implies that the acceleration is continuous].

- C1: first derivatives equal.
- Cn: nth derivatives are equal.

As their names imply, geometric continuity requires the geometry to be continuous, while parametric continuity requires the underlying parameterization to be continuous as well. Parametric continuity of order  $n$  implies geometric continuity of order  $n$ , but not vice-versa.

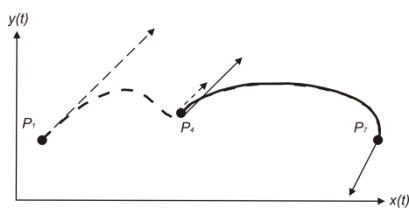
Hermite-curves

The curve segments are specified in this method through the end points  $P1$  and  $P4$  and their tangent vectors  $R1$  and  $R4$ .

$$G = \begin{bmatrix} P_1 \\ P_2 \\ P_3 \\ P_4 \end{bmatrix} \text{ and } M = \begin{bmatrix} 2 & -2 & 1 & 1 \\ -3 & 3 & -2 & -1 \\ 0 & 0 & 1 & 0 \\ 1 & 0 & 0 & 0 \end{bmatrix} \quad \text{Equation 5}$$

$$Q(t) = B \cdot G = (2t^3 - 3t^2 + 1) P1 + (-2t^3 + 3t^2) P4 + (t^3 - 2t^2 + t) R1 + (t^3 - t^2) R4 \quad \text{Equation 6}$$

Due to its nature, the hermite curve modelling method can just by the use of extra constraints, keep between the 2 connected curves the 1<sup>st</sup> parametric continuity parameter (C1) (normally, the first derivative in the curve's join point is not equal for both sides, but proportional, as the Equation 7 and Figure 6 show).



$$\begin{bmatrix} P_1 \\ P_4 \\ R_1 \\ R_4 \end{bmatrix} = \begin{bmatrix} P_4 \\ P_7 \\ k.R_4 \\ R_7 \end{bmatrix}, k > 0$$

**Figure 6: joint point (P4) between 2 hermite curves, and the difference between the derivatives in this point (R4 and k\*R4)**

**Equation 7**

Berzier-Curves

The Berzier curves are the curve segments through the end points  $P1$  and  $P4$  and through the control points  $P2$  and  $P3$ . Its Basis matrix and its result polynomial are:

$$B = \begin{bmatrix} -1 & 3 & -3 & 1 \\ 3 & -6 & 3 & 0 \\ -3 & 3 & 0 & 0 \\ 1 & 0 & 0 & 0 \end{bmatrix} \quad \text{Equation 8}$$

$$Q(t) = B \cdot G = (1-t)^3 P_1 + 3t(1-t)^2 P_2 + 3t^2(1-t) P_3 + t^3 P_4 \quad \text{Equation 9}$$

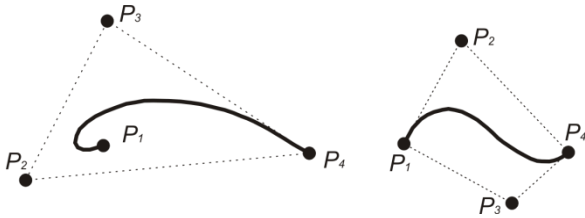


**Figure 7: the berzier curve never pass outside the convex hull formed by the four control points, but it is not necessary that all control points stay on this hull**

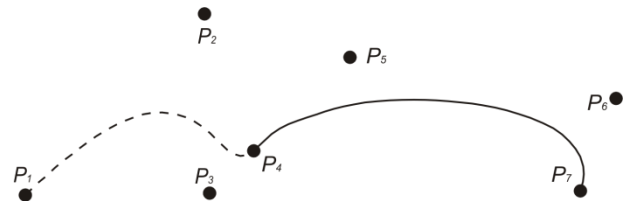


**Figure 8: two berzier curves, in P4 joined**

As by the hermite curve modelling method, the berzier method, due to its nature, can just by the use of extra constraints, keep between the 2 connected curves the 1<sup>st</sup> parametric continuity parameter (C1) (the first derivative in the curve's joint point is not equal for both sides).

### B-Spline curves

The B-Spline curves are the curve segments through the control points P1, P2, P3 and P4. In the special case of the uniform non-rational B-Spline, the Basis matrix and its result polynomial are:

$$B = \begin{bmatrix} 0 & 1 & 4 & 1 \\ 0 & 3 & 0 & 3 \\ 0 & 3 & 6 & 3 \\ 1 & 3 & 3 & 1 \end{bmatrix} \quad \text{Equation 10}$$

$$Q(t) = B \cdot G = (1-t)^3 P_1 + (3t^3 - 6t^2 + 4) P_2 + (-3t^3 + 3t^2 + 3t + 1) P_3 + t^3 P_4 \quad \text{Equation 11}$$

A B-Spline is composed of  $m+1$  control points and  $m-2$  segments. In the Figure 9 a B-Spline with  $m = 9$  is shown. These curves respect also the convex hull principle, as the Berzier curves (see Figure 7).

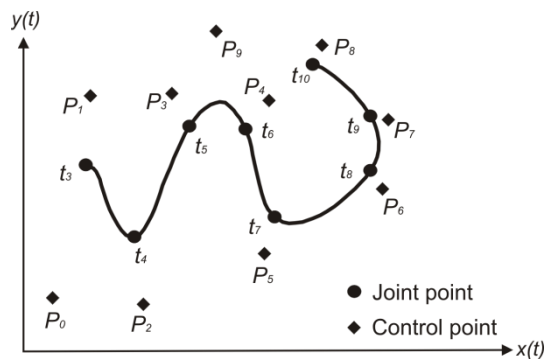


**Figure 9: Example of a B-Spline curve**

This method has a parametric continuity until the second derivative (C2), which means that the curvature values are continuous over the curve.

The Method chosen for the software was the uniform non-rational B-Spline method, as it is the method that matches the requirement of a continuous curvature over the curve.

Based on some tests of the software with real measured shapes, it was seen that for some measurements with a relative high SNR (signal to noise ratio), some outlier points influenced strongly the generated curve and consequently its curvature graphic. This influence can be seen in the generated shape of the Figure 10.

Considering this issue, a parameter was developed, which has as purpose the smoothing of the generated B-Spline curves.

As explained in the earlier sections, the calculation of B-Spline curves is based on a set of 4 control points. And the idea for the smooth parameter was to take not every measured point, but 4 points of a pre-determined length. The Length, which the software uses for the smoothing process, is the distance between every point. A example is shown in the Figure 11.

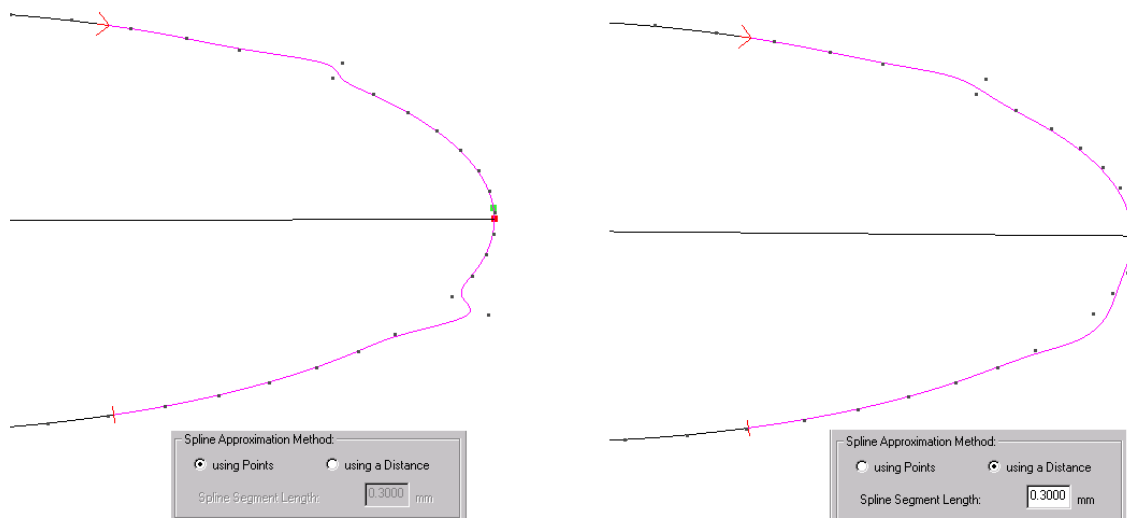


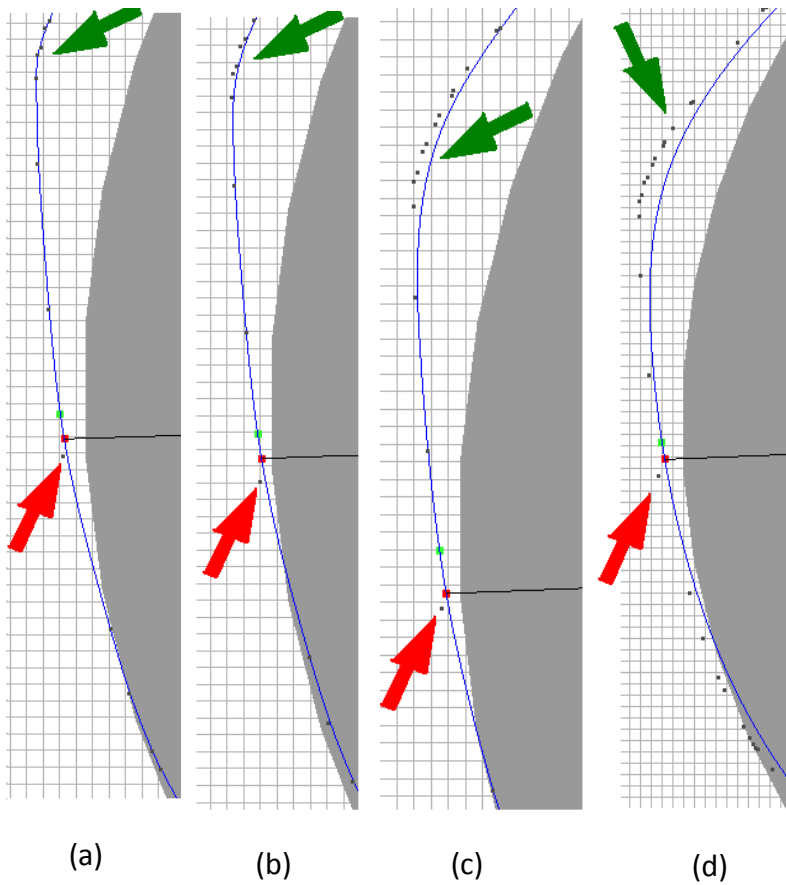
**Figure 10: Influence of outliers in the reconstruction of a blade edge**

The case, in which the defined length is between points, is not an issue, due to the fact, that a polynomial is fitted through the points, so the exact length can be extracted.

A comparison between the error added by the calculation of the B-Spline curve based on all points and using the smoothed parameters was carried out. The results show, that for a relative to the blade thickness small approximation Length, the error added in the B-Spline resultant curves is still negligible (max. error difference between the approx. in A, B and C).



**Figure 11: smooth parameter**



- Smoothing process of a blade:

- a) all points;
- b) approx. Length = 0,1mm;
- c) approx. Length = 0,2mm;
- d) approx. Length = 0,5mm;

- max. Error:

- a) 7,61 $\mu$ m;
- b) 6,31 $\mu$ m;
- c) 7,7 $\mu$ m;
- d) 18,4 $\mu$ m;

\* the approx. Length is relativ to a blade with a thickness of 2,5 mm

**Figure 12: smoothing parameter comparison**

### 2.5 Curvature calculation

The definition of curvature in geometry and mathematic is the direction's change per unit length. In other words, the curvature from a curve in a certain point P describes the curve's deviation in the immediate adjacencies from a straight line.  $\vec{r}(s)$  is the position vector of a point in a curve as a function of the arc length  $s$ . The curvature  $\kappa$  of a curve is then defined as:

$$\kappa = \left| \frac{d^2 \vec{r}}{ds^2} \right| \quad \text{Equation 12}$$

The curvature value of a straight line is always zero and of a circle is always the mathematical inverse of its radius. In other curves this values change for every point.

In the case of a plane curve the curvature is also defined as  $\kappa = \left| \frac{d\alpha}{ds} \right|$ , where  $\alpha$  is the angle of inclination (see Figure 13).

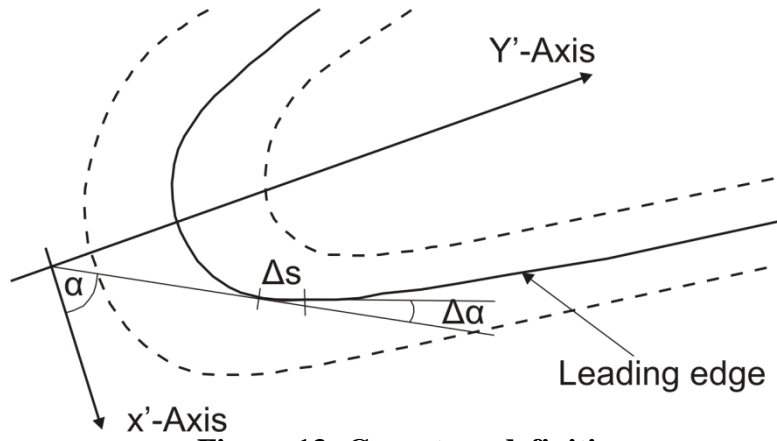


Figure 13: Curvature definition

And also coming from the definition from the Equation 13 and the Figure 13 the following equations are gain: (where  $\alpha$  is the tangential angle and  $s$  is the arc length)

$$\kappa = \left| \frac{d\alpha}{ds} \right| = \left| \frac{d\alpha/dt}{ds/dt} \right| = \left| \frac{d\alpha/dt}{\sqrt{(dx/dt)^2 + (dy/dt)^2}} \right| = \left| \frac{d\alpha/dt}{\sqrt{(x')^2 + (y')^2}} \right| \quad (1)$$

$$\tan \alpha = \frac{dy}{dx} = \frac{dy/dt}{dx/dt} = y'/x' \Rightarrow \frac{d(\tan \alpha)}{dt} = \sec^2 \alpha \cdot \frac{d\alpha}{ds} = \frac{x' \cdot y'' - x'' \cdot y'}{x'^2} \quad (2)$$

$$\frac{d\alpha}{ds} = \frac{1}{\sec^2 \alpha} \cdot \frac{d(\tan \alpha)}{dt} = \frac{1}{1 + \tan^2 \alpha} \cdot \frac{x' \cdot y'' - x'' \cdot y'}{x'^2} = \frac{1}{1 + y'^2/x'^2} \cdot \frac{x' \cdot y'' - x'' \cdot y'}{x'^2} = \frac{x' \cdot y'' - x'' \cdot y'}{x'^2 + y'^2} \quad (3)$$

$$\text{Joining (1) and (3)} \rightarrow \kappa = \left| \frac{x' \cdot y'' - x'' \cdot y'}{(x'^2 + y'^2)^{3/2}} \right| = \left| \frac{y''}{(1 + y'^2)^{3/2}} \right| \quad \text{Equation 14}$$

In least squares (LS) estimation, the unknown values of the parameters,  $\beta_0, \beta_1, \dots$ , in the regression function,  $f(\vec{x}; \vec{\beta})$ , are estimated by finding numerical values for the parameters that minimize the sum of the squared deviations between the observed responses and the functional portion of the model. Mathematically, the least (sum of) squares criterion that is minimized to obtain the parameter estimates is

$$Q = \sum_{i=1}^n [y_i - f(\vec{x}_i; \vec{\beta})]^2$$

As previously noted,  $\beta_0, \beta_1, \dots$  are treated as the variables in the optimization and the predictor variable values,  $x_1, x_2, \dots$  are treated as coefficients. To emphasize the fact that the estimates of the parameter values are not the same as the true values of the parameters, the estimates are denoted by  $\beta_0, \beta_1, \dots$ . For linear models, the least squares minimization is usually done analytically using calculus. For nonlinear models, on the other hand, the minimization must almost always be done using iterative numerical algorithms.

Based on this description and on the assumption, that the curvature at a given point P has a magnitude equal to the reciprocal of the radius of an osculating circle (a circle that closely touches the curve at the given point, its center shaping the curve's evolute, see ) ( $\kappa = 1/\text{Radius}$ ), an algorithm was written using the measured points to fit a circle, and with its radius to calculate the curvature of the middle point of this region.

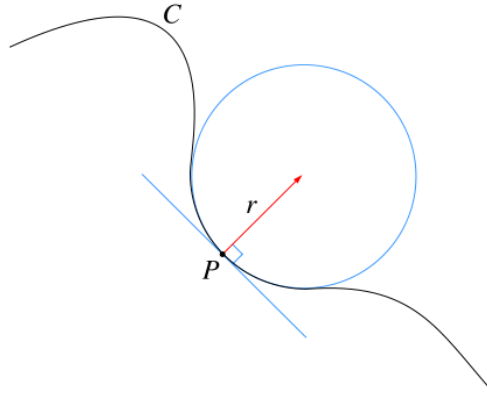


Figure 14: circle fit - osculation circle

## 2.6 Initial Blade Inspect Testing

Three function were tested on the software with the aim of testing the accuracy of the method.

a)  $f(x) = 5 \cdot x^2$

$$f(x)'' = 10 \text{ and } f(x)' = 10 \cdot x \rightarrow \kappa = \left| \frac{y''}{(1 + y'^2)^{3/2}} \right| \rightarrow \kappa = \frac{10}{(1 + 100 \cdot x^2)^{3/2}}$$

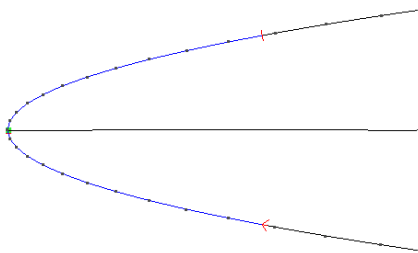


Figure 15: generated parabola-shaped edge

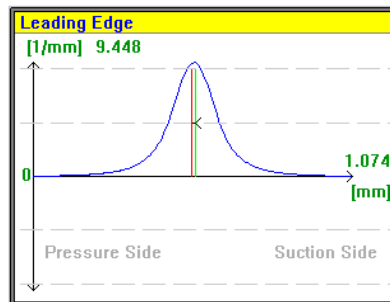


Figure 16: resulted curvature graphic, using blade inspect

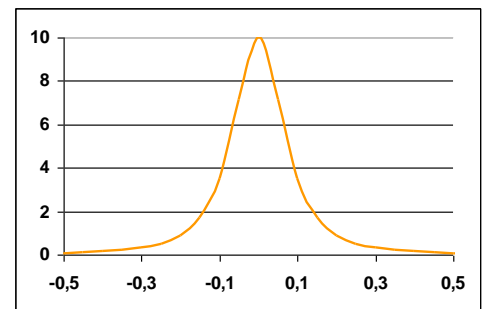


Figure 17: resulted curvature graphic, based on a mathematical software

b)  $x = 0,5 \cdot \cos(\theta)$  and  $y = 1,5 \cdot \sin(\theta)$  (3 to 1 ellipse)

$$x'' = -0,5 \cdot \cos(\theta) \text{ and } x' = -0,5 \cdot \sin(\theta) / y'' = -1,5 \cdot \sin(\theta) \text{ and } y' = 1,5 \cdot \cos(\theta) \rightarrow$$

$$\kappa = \left| \frac{x' \cdot y'' - x'' \cdot y'}{(x'^2 + y'^2)^{3/2}} \right|$$

$$\rightarrow \kappa = \left| \frac{0,75 \cdot \sin^2(\theta) + 0,75 \cdot \cos^2(\theta)}{(0,25 \cdot \sin^2(\theta) + 2,25 \cdot \cos^2(\theta))^{\frac{3}{2}}} \right| \rightarrow \kappa = \left| \frac{0,75}{(0,25 \cdot \sin^2(\theta) + 2,25 \cdot \cos^2(\theta))^{\frac{3}{2}}} \right|$$

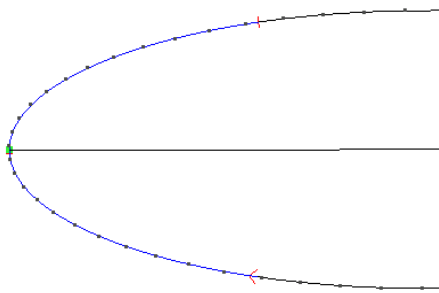


Figure 18: generated elliptical-shaped edge

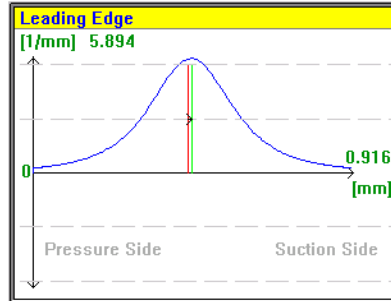


Figure 19: resulted curvature graphic, using blade inspect

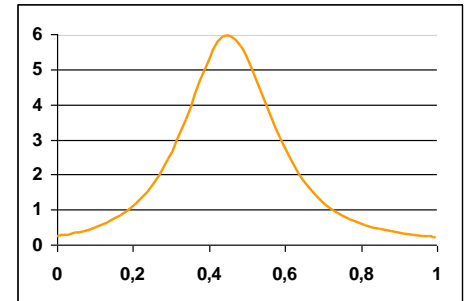


Figure 20: resulted curvature graphic, based on a mathematical software

c)  $x = 0,5 \cdot \cos(\theta)$  and  $y = 0,5 \cdot \sin(\theta)$  (circle)

$$x'' = -0,5 \cdot \cos(\theta) \quad \text{and} \quad x' = -0,5 \cdot \sin(\theta) \quad / \quad y'' = -0,5 \cdot \sin(\theta) \quad \text{and} \quad y' = 0,5 \cdot \cos(\theta) \quad \rightarrow$$

$$\kappa = \left| \frac{x' \cdot y'' - x'' \cdot y'}{(x'^2 + y'^2)^{\frac{3}{2}}} \right|$$

$$\rightarrow \kappa = \left| \frac{0,25 \cdot \sin^2(\theta) + 0,25 \cdot \cos^2(\theta)}{(0,25 \cdot \sin^2(\theta) + 0,25 \cdot \cos^2(\theta))^{\frac{3}{2}}} \right| \rightarrow \kappa = \left| \frac{0,25}{(0,125)} \right| = 2$$

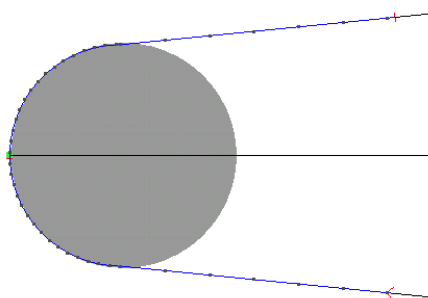


Figure 21: generated circle-shaped edge

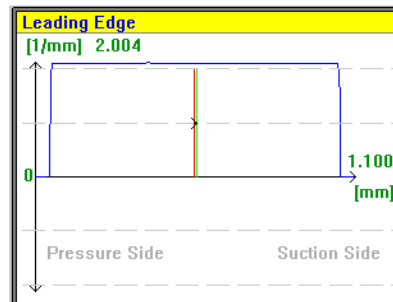


Figure 22: resulted curvature graphic, using blade inspect

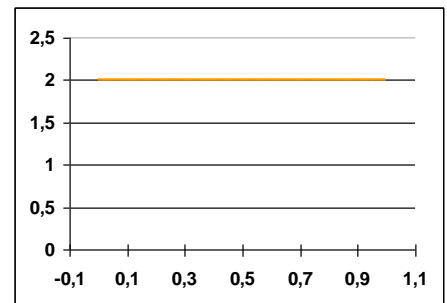


Figure 23: resulted curvature graphic, based on a mathematical software

Based on the results showed above, it was concluded that the circle fit method is very dependent on the point density, as it was expected, because the quality of the fits is dependent on the number of points selected and on the number of points for describing a determined area. This dependency is easy to be seen on sharp-shaped edges, were a stronger curvature change happens and the method can just follow correctly with the use of a higher point density. (see Figure 25, Figure 26, Figure 19 and Figure 29. This method uses the curvature equation for plane curves already shown at the beginning of the section, and the polynomial created by B-Spline (UNRBS)



method. The B-Spline algorithm returns for every set of selected points a polynomial, which describes the curve position for each axis (x, y, z) as a function of the arc length. As the curvature equation requires a polynomial description of the axis positions, it is possible to develop a curvature polynomial for every set of selected points.

Method:  $Q(t) = \begin{bmatrix} x(t) \\ y(t) \\ z(t) \end{bmatrix}, \quad P_n = \begin{bmatrix} x_n \\ y_n \\ z_n \end{bmatrix} \rightarrow$

$$\begin{aligned} x(t) &= (1-t)^3 \cdot x_1 + (3t^3 - 6t^2 + 4) \cdot x_2 \\ &\quad + (-3t^3 + 3t^2 + 3t + 1) \cdot x_3 + t^3 \cdot x_4 \\ y(t) &= (1-t)^3 \cdot y_1 + (3t^3 - 6t^2 + 4) \cdot y_2 \\ &\quad + (-3t^3 + 3t^2 + 3t + 1) \cdot y_3 + t^3 \cdot y_4 \end{aligned} \rightarrow$$

$$\kappa = \left| \frac{x' \cdot y'' - x'' \cdot y'}{(x'^2 + y'^2)^{3/2}} \right|$$

Three function were tested on the software with the aim of testing the accuracy of the method.

a)  $f(x) = 5 \cdot x^2$

$$f(x)'' = 10 \text{ and } f(x)' = 10 \cdot x \rightarrow \kappa = \left| \frac{y''}{(1 + y'^2)^{3/2}} \right| \rightarrow \kappa = \frac{10}{(1 + 100 \cdot x^2)^{3/2}}$$

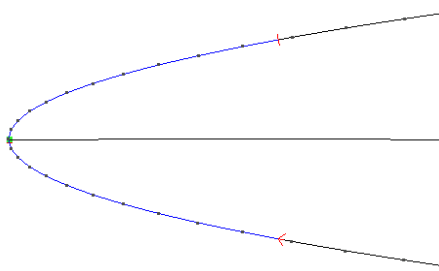


Figure 24: generated parabola-shaped edge

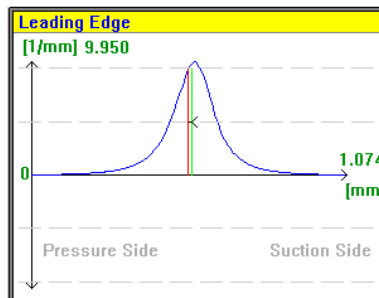


Figure 25: resulted curvature graphic, using blade inspect

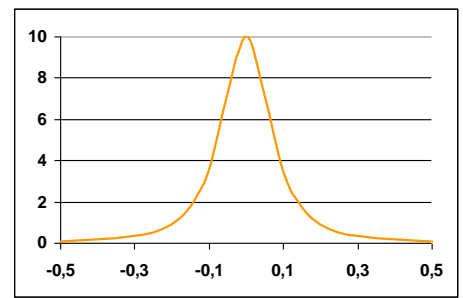


Figure 26: resulted curvature graphic, based on a mathematical software

b)  $x = 0,5 \cdot \cos(\theta)$  and  $y = 1,5 \cdot \sin(\theta)$  (3 to 1 ellipse)

$$x'' = -0,5 \cdot \cos(\theta) \text{ and } x' = -0,5 \cdot \sin(\theta) \quad / \quad y'' = -1,5 \cdot \sin(\theta) \text{ and } y' = 1,5 \cdot \cos(\theta) \rightarrow$$

$$\kappa = \left| \frac{x' \cdot y'' - x'' \cdot y'}{(x'^2 + y'^2)^{3/2}} \right|$$

$$\rightarrow \kappa = \left| \frac{0,75 \cdot \sin^2(\theta) + 0,75 \cdot \cos^2(\theta)}{(0,25 \cdot \sin^2(\theta) + 2,25 \cdot \cos^2(\theta))^{3/2}} \right| \rightarrow \kappa = \left| \frac{0,75}{(0,25 + 2 \cdot \cos^2(\theta))^{3/2}} \right|$$

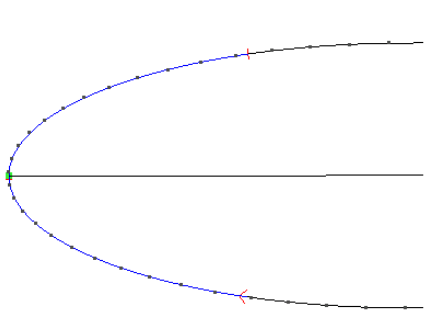


Figure 27: generated elliptical-shaped edge

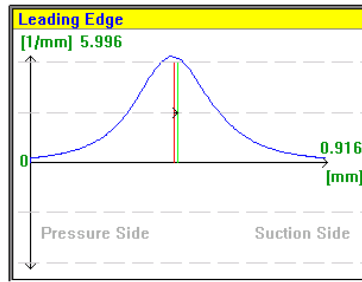


Figure 28: resulted curvature graphic, using blade inspect

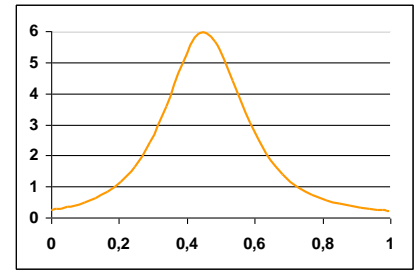


Figure 29: resulted curvature graphic, based on a mathematical software

c)  $x = 0,5 \cdot \cos(\theta)$  and  $y = 0,5 \cdot \sin(\theta)$  (circle)

$$x'' = -0,5 \cdot \cos(\theta) \quad \text{and} \quad x' = -0,5 \cdot \sin(\theta) \quad / \quad y'' = -0,5 \cdot \sin(\theta) \quad \text{and} \quad y' = 0,5 \cdot \cos(\theta) \quad \rightarrow$$

$$\kappa = \left| \frac{x' \cdot y'' - x'' \cdot y'}{(x'^2 + y'^2)^{3/2}} \right|$$

$$\rightarrow \kappa = \left| \frac{0,25 \cdot \sin^2(\theta) + 0,25 \cdot \cos^2(\theta)}{(0,25 \cdot \sin^2(\theta) + 0,25 \cdot \cos^2(\theta))^{3/2}} \right| \rightarrow \kappa = \left| \frac{0,25}{(0,125)} \right| = 2$$

Based on the results shown, it was concluded that the method is only lightly dependent on the point density. What is also to be concluded based on the method equations, as the software has a function that describes the curvature, and in this point less dependent of the point density. Another point that improves the accuracy is that this method estimates the curvature value directly from a description of the points and not through a fitting process, what eliminates iteration processes and with it the possibility of bad convergences.

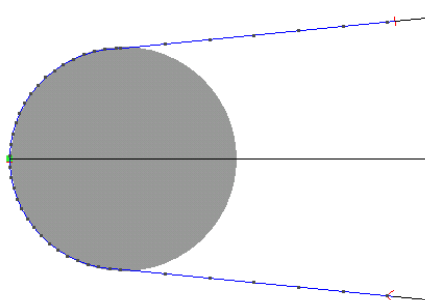


Figure 30: generated circle-shaped edge

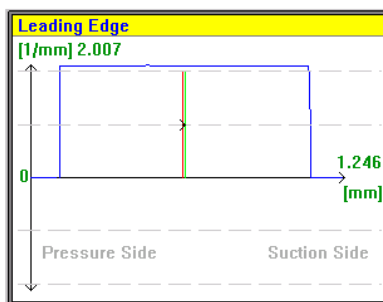


Figure 31: resulted curvature graphic, using blade inspect

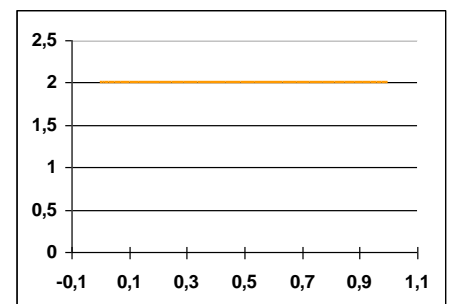


Figure 32: resulted curvature graphic, based on a mathematical software

## 2.7 Smoothing parameters

With the aim of eliminating noise from curvature values, which are calculated based on measured blade edges, a curvature smooth parameter was created. The mathematical base of this

parameter is similar to the other smooth parameter. As explained in the earlier sections, the calculation of B-Spline curves is based on a set of 4 control points, and the idea for the smooth parameter was to take not every measured point, but 4 points of a pre-determined length. The Length, which the software uses for the smoothing process, is the distance between every point. Having the B-Spline polynomial the curvature can be calculated, and as the polynomial is already smoothed the curvature will also be smoothed (see figure 11). Using this parameter just the curvature values will be smoothed, the blade edge shape will not suffer any change. In the Picture below it is shown how this parameter works on a measured blade edge.

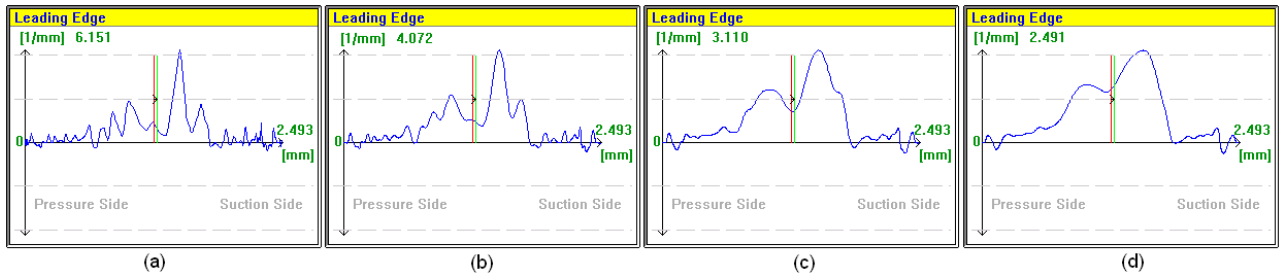


Figure 33: curvature graphics smoothed with a length of (a) 0,01mm (b) 0,2mm (c) 0,4mm (d) 0,6mm

The curvature smooth parameter influence the shape of a curvature graphic, smoothing the sharp transitions, as it can be seen in the pictures below. If the blade doesn't have a sharp edge, the max curvature value stays close to its magnitude, oscillating depending on the selected regions (Figure 34).

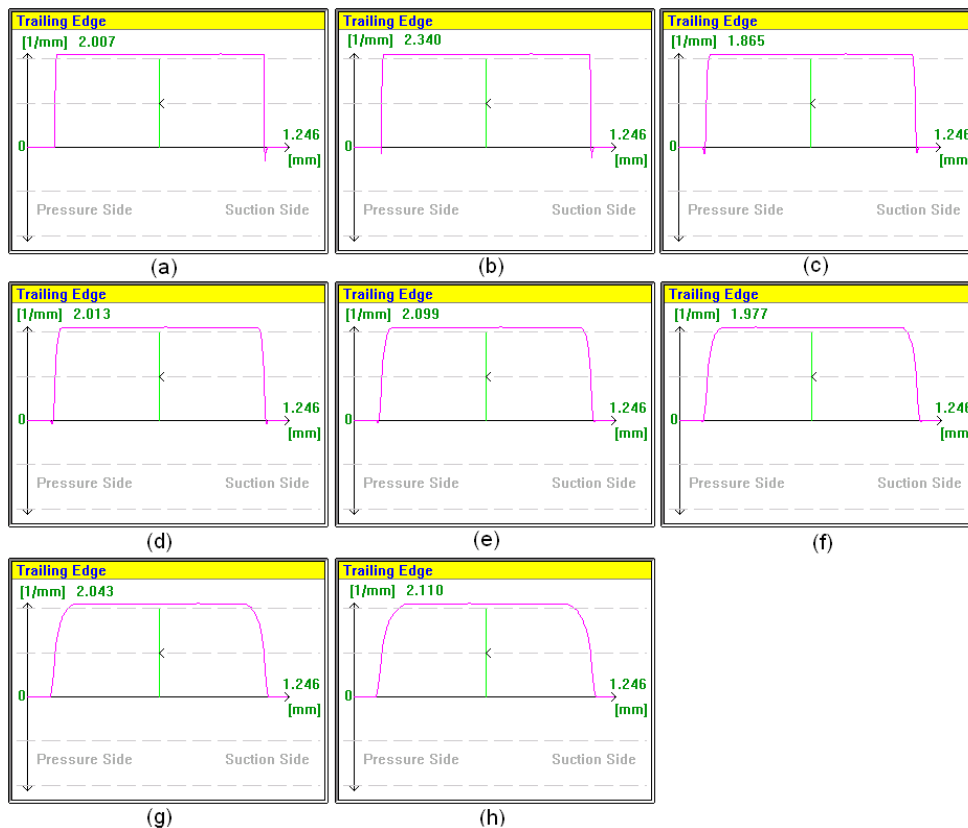


Figure 34: curvature graphics of a circle-shaped edge for different smooth lengths, (a) 0,01mm (b) 0,1mm (c) 0,2mm (d) 0,3mm (e) 0,4mm (f) 0,5mm (g) 0,6mm (h) 0,7mm

The edge shape smooth parameter has also an influence on the curvature graphic, as this parameter changes the current loaded shape, changing also the curvature values related to it. (see pictures below).

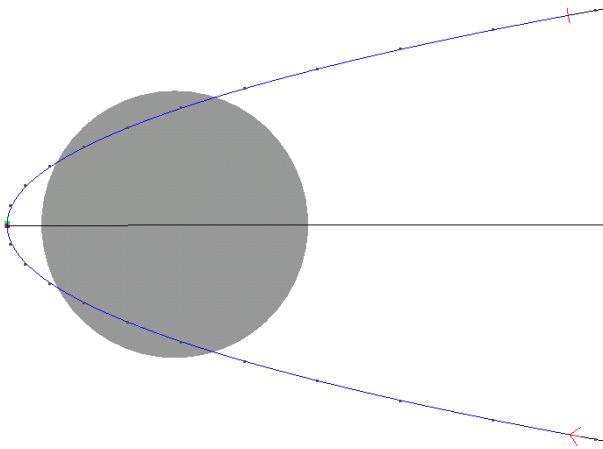


Figure 35: edge shape with edge smooth parameter length equal to 0,01mm.

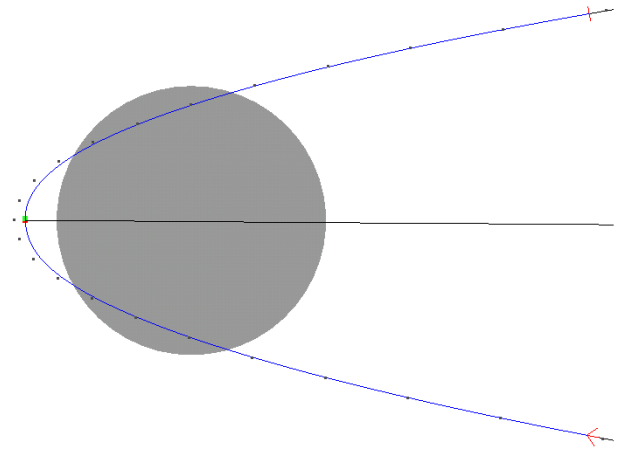


Figure 38: edge shape with edge smooth parameter length equal to 0,4mm.



Figure 36: curvature graphic of the shape shown in

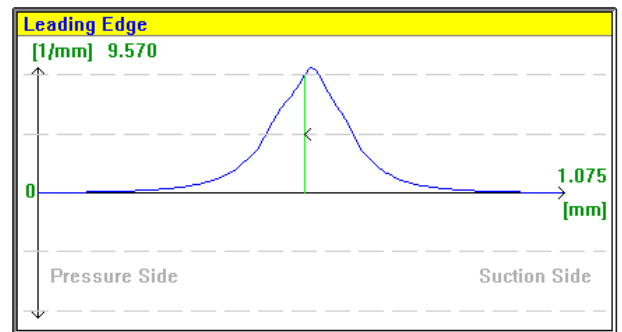


Figure 39: curvature graphic of the shape shown in

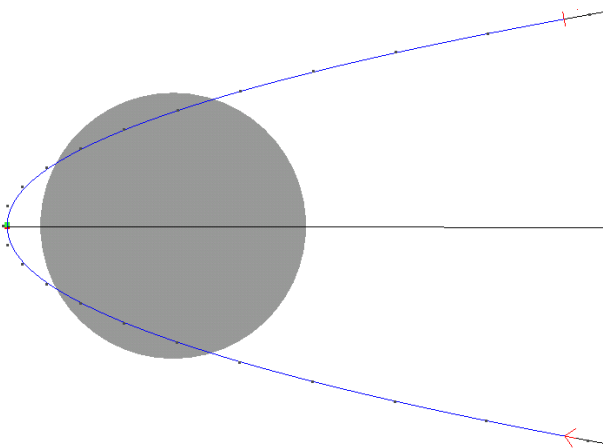


Figure 37: edge shape with edge smooth parameter length equal to 0,2mm.

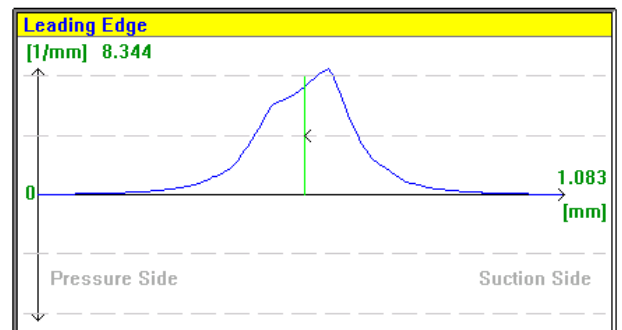


Figure 40: curvature graphic of the shape shown in

## 2.8 Conclusions and perspectives

This document explained all the mathematics behind the pre-processing stage of the software blade inspect, which comprehend the curve modelling method and the curvature calculation. As well as gave a proof of the accuracy and reliability of those.

One perspective of improvement of this process, would be the automation of these parameters, based on the minimization of the shape error and of the curvature graphic noise.

### 3. Curvature Tolerancing implementation method

#### 3.1 Introduction

The current version of the Software Blade Inspect makes use of a sentencing criteria, which is based on tolerance bands in curvature plots of leading / trailing edge shapes, as the figure 1 shows.

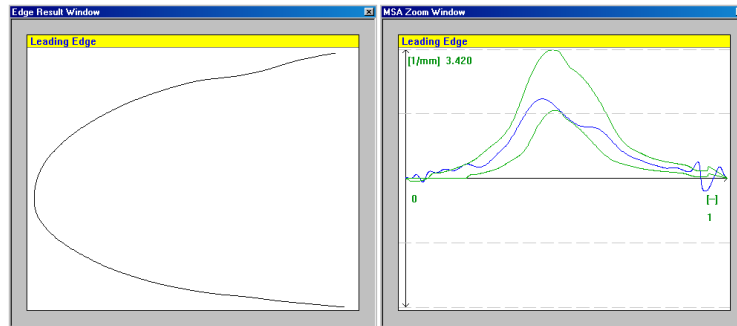


**Figure 1: Edge Shape, its Curvature plot (blue) and the generated Tolerance Bands**

The Curvature based tolerance bands were generated related to a set of blades, which were assessed by Dave Lambie (section AU and AZ). All assessed edge's curvature plots were put together and the upper and lower envelope of the accepted edges was used, as well as the nominal curvature plot, in order to generate the tolerance (a better explanation is on the technical reports related to the project). The result of the tolerance tests showed, that a single tolerance band for all sections does not achieve an appropriate classification percentage. Fact that leads the solution to a set of tolerance bands for different blade sections. The Decision related to the number of tolerance bands will be carried out with regard to a new assessment from the engineering department of Bristol, which will also cover the section AV, AW, AX and AY. The whole procedure from the tolerance creation until the results is explained in the figure 2 and in the next sections.

#### 3.2 Tolerance creation

The Tolerance creation followed the methods explained in the report "Automated assessment of blade's leading edge profiles – Sentencing criteria". The parameter values set for the tolerance to fit the envelope of the assessed group of blade edge's curvature is shown below.

- Method 1:

**Table 0-1: tolerance generation, parameters for AZ**

	Suction				Pressure			
	Curvature	Y offset	Skew	scale	Curvature	Y offset	Skew	scale
upper tolerance band	2	1	-0,1	100	3,4	0	0	160
Lower tolerance band	1,75	-0,16	-0,02	85	1,5	0,05	0,015	95

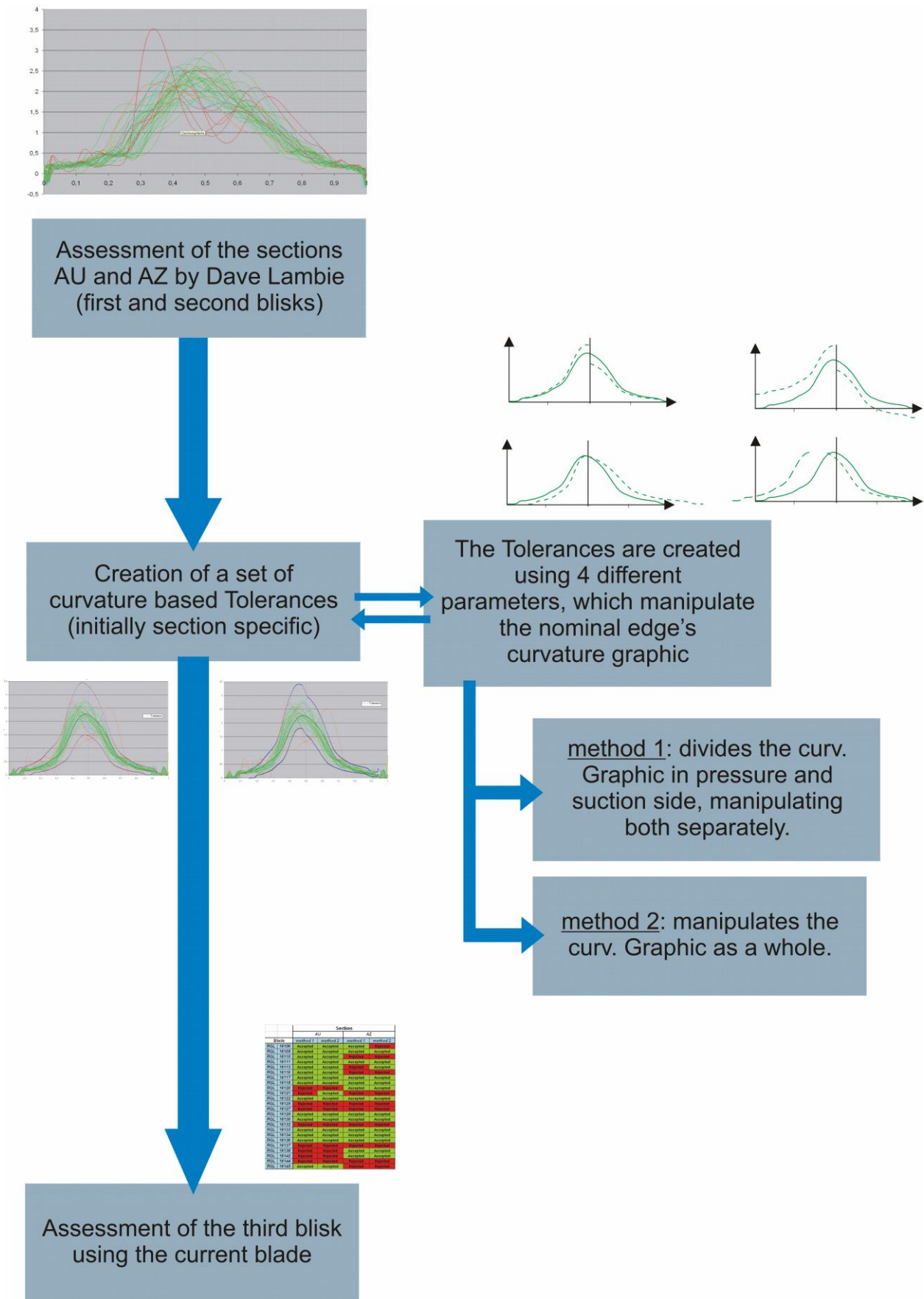


Figure 0: Test sequence



	Suction				Pressure			
	Curvature	Y offset	Skew	scale	Curvature	Y offset	Skew	scale
upper tolerance band	3,65	0,2	-0,049	85	3,45	0,3	0,008	86
Lower tolerance band	2,4	-0,16	-0,019	80	1,98	0,05	0,005	78

**Table 2: tolerance generation, parameters for AU**

- Method 2:

	whole blade			
	Curvature	Y offset	Skew	scale
upper tolerance band	3,4	0,35	-0,03	142
Lower tolerance band	1,94	-0,4	0,013	120

**Table 3: tolerance generation, parameters for AZ**

	whole blade			
	Curvature	Y offset	Skew	scale
upper tolerance band	3,8	0,1	-0,024	107
Lower tolerance band	2,45	-0,3	-0,015	90

**Table 4: tolerance generation, parameters for AU**

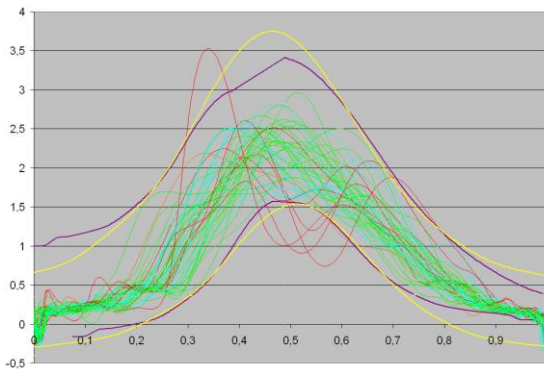


**Figure 3: AZ Tolerance bands (method 1 in purple and method 2 in yellow)**

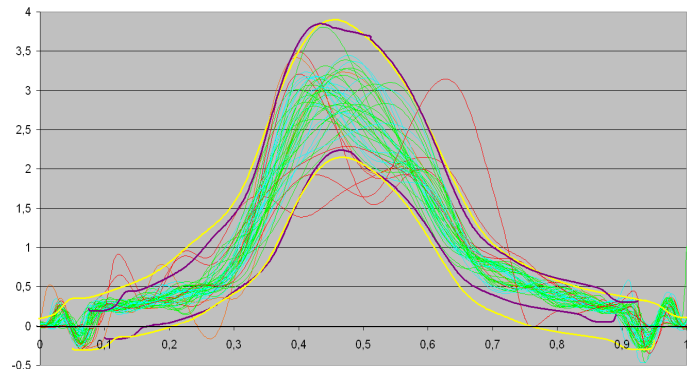


**Figure 4: AU Tolerance bands (method 1 in purple and method 2 in yellow)**

### 3.3 Blisk assessment using tolerances in the curvature graphic

Using the tolerance bands generated as explained before, the Blisk has been assessed by the software *blade inspect*. The Table 5 show the results for every blade from the mentioned blisk.

		Section			
		AU		AZ	
Blade		method 1	method 2	method 1	method 2
RGL	16106	Accepted	Accepted	Accepted	Rejected
RGL	16109	Accepted	Accepted	Accepted	Accepted
RGL	16110	Accepted	Accepted	Rejected	Rejected
RGL	16111	Accepted	Accepted	Accepted	Accepted
RGL	16113	Accepted	Accepted	Rejected	Accepted
RGL	16116	Accepted	Accepted	Rejected	Rejected
RGL	16117	Accepted	Accepted	Accepted	Accepted
RGL	16118	Accepted	Accepted	Accepted	Accepted
RGL	16120	Rejected	Rejected	Accepted	Accepted
RGL	16121	Rejected	Accepted	Rejected	Rejected
RGL	16122	Accepted	Accepted	Accepted	Accepted
RGL	16125	Rejected	Rejected	Rejected	Rejected
RGL	16127	Rejected	Rejected	Rejected	Rejected
RGL	16129	Accepted	Accepted	Accepted	Accepted
RGL	16130	Accepted	Accepted	Accepted	Accepted
RGL	16132	Rejected	Rejected	Rejected	Rejected
RGL	16133	Accepted	Accepted	Accepted	Accepted
RGL	16134	Accepted	Accepted	Accepted	Accepted
RGL	16136	Accepted	Accepted	Accepted	Accepted
RGL	16137	Rejected	Rejected	Rejected	Rejected
RGL	16138	Rejected	Rejected	Accepted	Accepted
RGL	16142	Rejected	Rejected	Accepted	Accepted
RGL	16144	Rejected	Rejected	Rejected	Rejected
RGL	16145	Accepted	Accepted	Rejected	Rejected

Table 5: Software assessment results

Some of the blades, which were rejected, are shown below with the respective relation between tolerance-curvature intersection and blade edge.

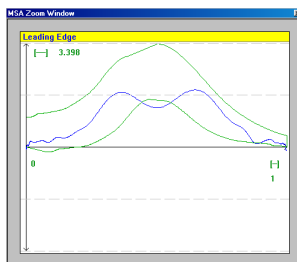


Figure 5: Blade 16145 AZ, tolerance - curvature intersection

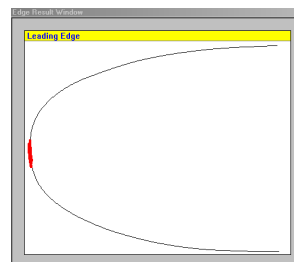


Figure 6: Blade 16145 AZ, blade edge

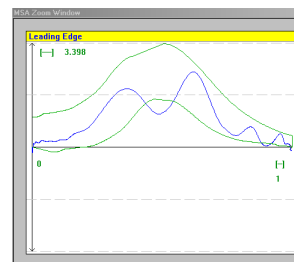


Figure 7: Blade 16132 AZ, tolerance - curvature intersection

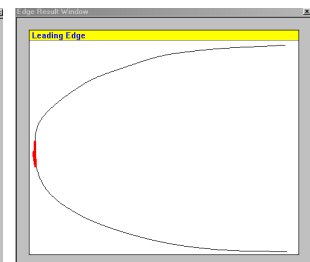
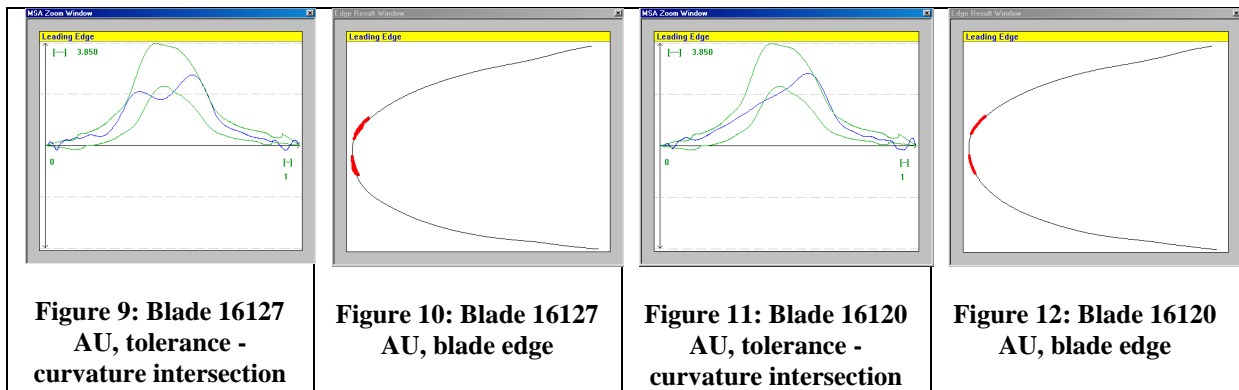


Figure 8: Blade 16132 AZ, blade edge



## 4. Automation demonstrator

### 4.1 Introduction

The automated leading edge assessment project as led to the creation of software package named blade inspect. The sentencing method consists of applying an upper and lower tolerance band to the rate of curvature of the leading edge (LE) profile. Using curvature as the output quantity, two types of analysis were developed. A non dimensional plot of curvature versus arc length (CVNAL) of the LE profile and the non dimensional plot of curvature versus thickness position (CVNTP). Some initial testing revealed that although the CVNTP method provides the user a better visual interpretation of the curvature at the LE tip, it can be sensitive to the way the thickness line is derived.

Synthetic blade sets containing variation representative of the manufacturing process were used to derive tolerance bands for the blisk. These were set on a section by section basis.

As part of the project milestones an automation demonstrator was required at pre production facility. This document will focus on three major aspects of this project:

- a) – Automation demonstrator
- b) – Tolerance band testing on the first ISR blisk
- c) - CVNAL vs CVNTP method for thinner blades

### 4.2 Automation demonstrator

The automation demonstrator consisted of updating the automation functionality already available in Blade Inspect so that a seamless integration with the current process.. The Figure-1 below shows the automation process used. It is worth noting that the DELCAM automation software available made the integration of BI with the manufacturing process easier. Blade Inspect was developed with two modes of operation, a user mode in which a trained inspector can assess individual LE's and a batch mode which allows for automated processing of  $n$  number of LE's.

Figure-2 shows the automation process flow diagram developed.

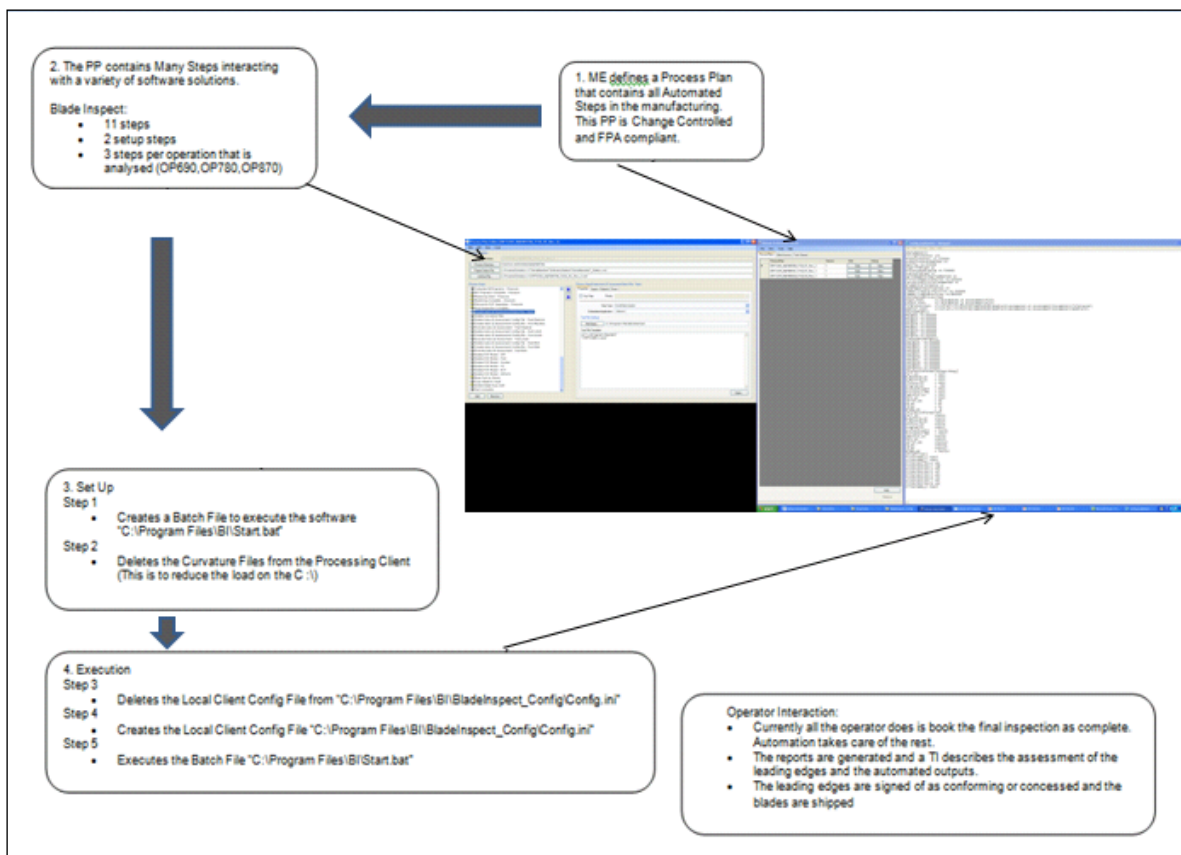


**Figure 2. Integration of Blade Inspect with Delcam**

The configuration file contains several parameters specific to both the mathematical analysis of the input data and the automation of the analysis. The Figure-3 below shows the mathematical analysis parameters and automation parameters. Automation parameters contain the paths for all input data requirements in BI.

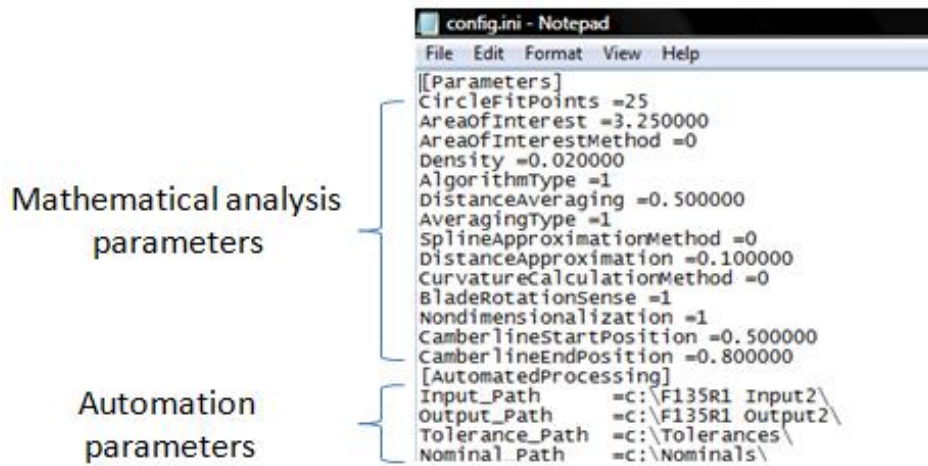


Figure 3. Integration of Blade Inspect with Delcam

Due to the possible naming convention for the input data, a set of filters (file naming filters, Figure-4) was developed so that the output data could be summarised at a later stage as a function of a filter such as "OP\_780", "OP\_690", or by blade "RGL155345". In addition blade section filters were also added due to different naming conventions for different engine blades.

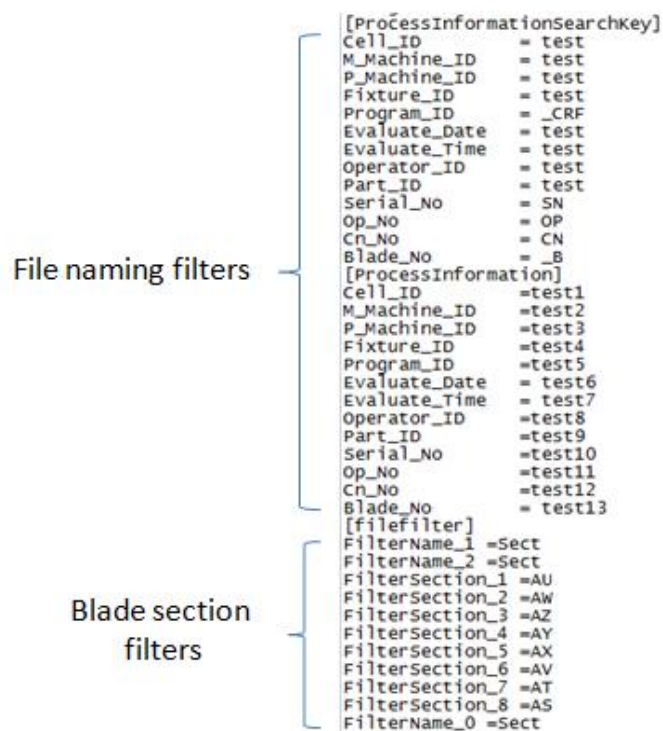


Figure 4. Integration of Blade Inspect with Delcam

During testing, having an editable configuration file allowed the user to set (create configuration files specific to an engine project) the correct parameters and filters for the

different types of input data. This step eliminated the need for human intervention making the output results consistent.

### 4.3 Tolerance band testing on first ISR blisk (CVNTP)

The tolerance bands used for the 1<sup>st</sup> blisk were derived using a tolerance master workbook where the nominal section leading edge curvature was modified using a set of parameters described in. Figure-5 shows the master workbook with a set of parameters values based on fans engineering Bristol assessment. Currently the generated tolerances have to be manually edited and converted to .txt files which are then called by Blade Inspect during the assessment.

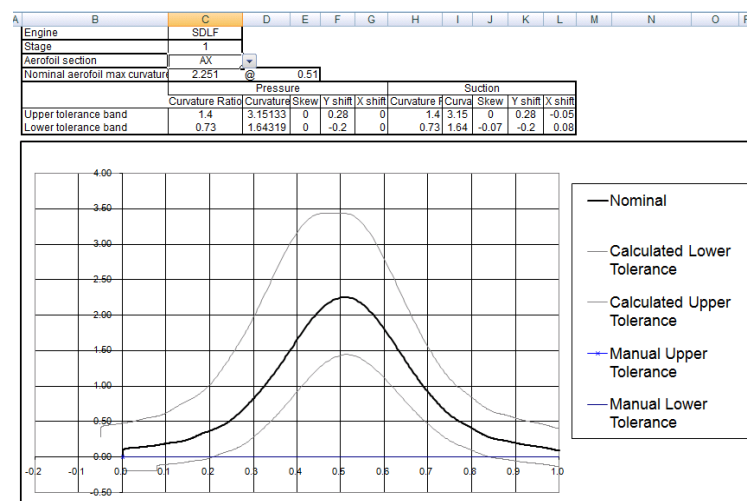


**Figure 5 – Master Workbook for tolerance generation.**

The Figure-6 below contains the summary results for all 1<sup>st</sup> ISR blades. The 1<sup>st</sup> ISR blisk consisted of 24 blades each with 8 sections named in the following manner:

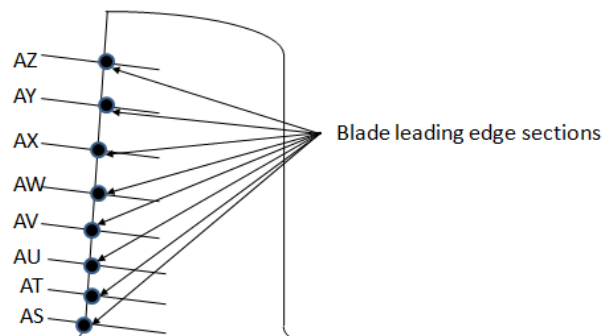


**Figure 6 – Master Workbook for tolerance generation.**

From the results obtained 52% of the blade sections were rejected while 48% were accepted. Sections AS and AT were always rejected but are less relevant than the 6

remaining sections. If both sections were not taken into account then 63% of the blade sections would have been accepted.

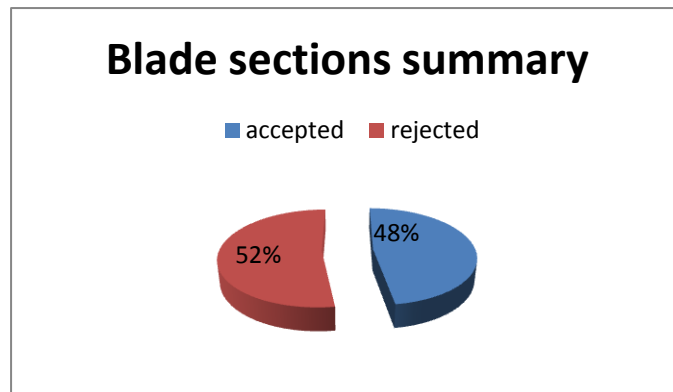


**Figure 7. Accepted/Rejected criteria performance**

The passing and failing percentages are a function of the tolerance bands set. By looking at the analysed blade section data in more detail it was clear that most blades were failing very close to the tolerance bands limits.

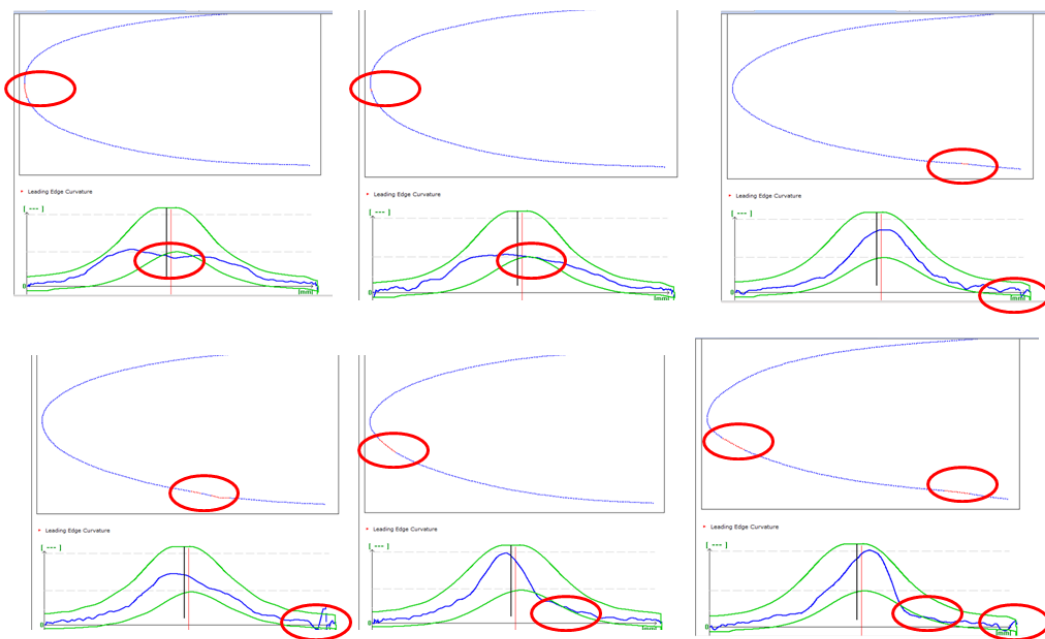


**Figure 2. Testing of the curvature Tolerancing method**

#### 4.4 CVNAL vs CVNTP method for thinner blades

Both curvature methods have been previously described. In this section both methods are compared using real blade data. Section 4.1 describes the CVNAL method in two modes of operation, CVNALULP mode which uses all the data points from the input data for the analysis and CVNALUTL mode in which the user sets the distance back from the leading edge to start the analysis. The same principle applies to the CVNTP method but due to the nature of the analysis in this method the impact of both modes will be described.

Two modes for the starting points of the analysis are available in BI. The first mode uses a camber line calculation to the input data to calculate a distance back from the LE. The distance can be set by the user and in the case of the engine project data presented in this document the value was set at 3.25mm. The second mode simply uses the last two points of the input data as the start and end points of the analysis.

Because the CVNAL method is a plot of curvature vs Arc Length, the differences between CVALULP and CVALUTL will be mainly scaling of the X axis in the curvature plot as seen on the figure below. This scaling effect will vary depending on the distance setting for TL and the consistency of the LP determination of the input point cloud data.

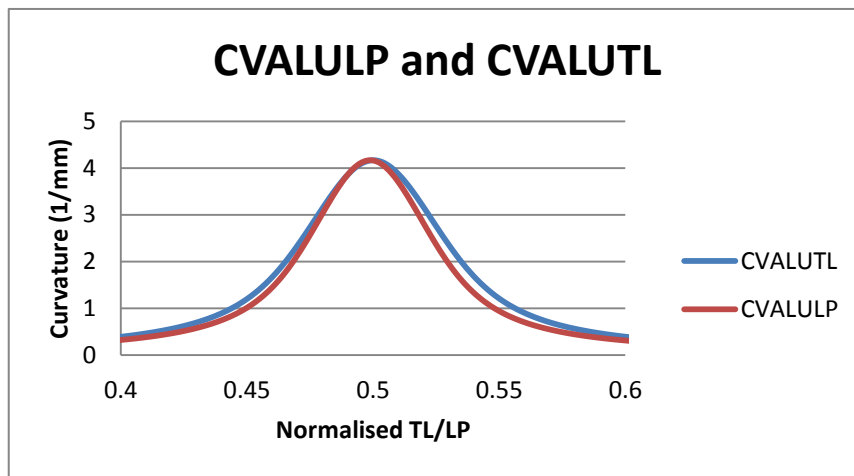


**Figure 3. Difference between the two modes for setting LE tip distance for start of the analysis.**

The following results were obtained when applying the method to a set of thinner blades belonging to a different blisk.

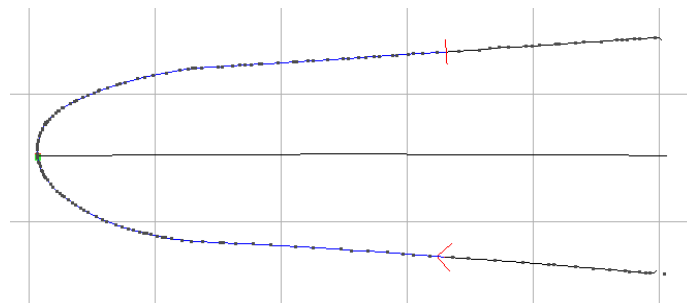


**Figure 4. Setting of LE tip distance option in blade inspect**



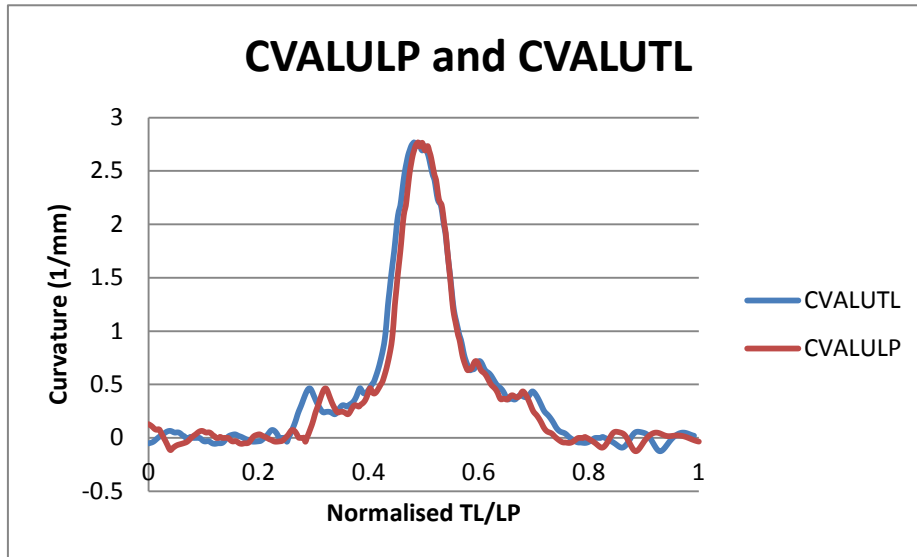


**Figure 5. Difference between the two modes for setting LE tip distance for start of the analysis.**

From the plot above it is clear that there is an effect of scaling as previously mentioned. There is also a difference in the angle between the first and last points on the two modes. This difference will cause a shift of curvature in the X axis which for the purpose of the analysis in this method can be considered negligible.

Below is a summary of the CVAL method applied to airfoils section AV. The curvature values are non-dimensionalised by  $\frac{1}{2}$  the measured thickness between the start and end points of the analysis.

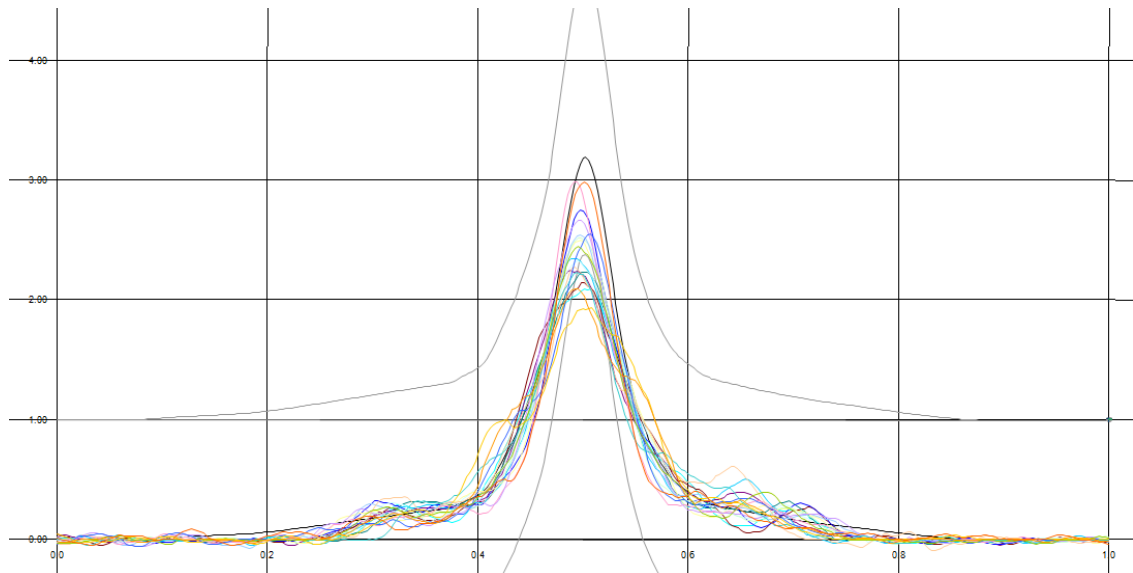


**Figure 6. Curvature plots section AV of multiple blades**

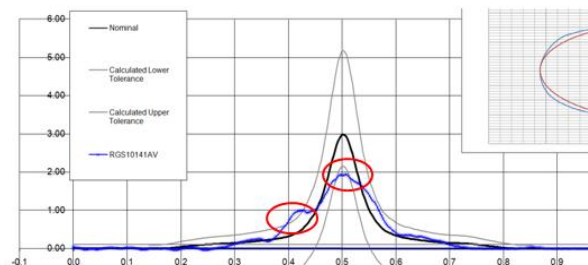
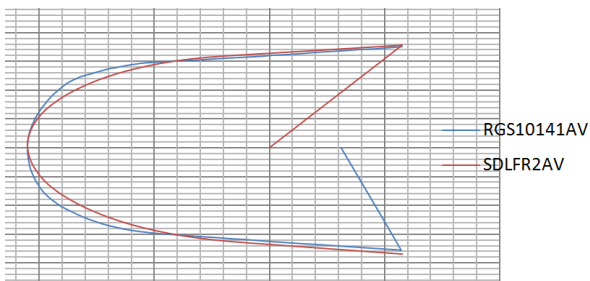
From the plot above it was clear that for the population of airfoil sections analysed, the peak curvature values had a range of 1.2 units. It was also clear that most of the curvature peaks for this set of results was below the nominal curvature of 3 units.

The range of peak curvature values can be converted to a range of leading edge tip radii using:

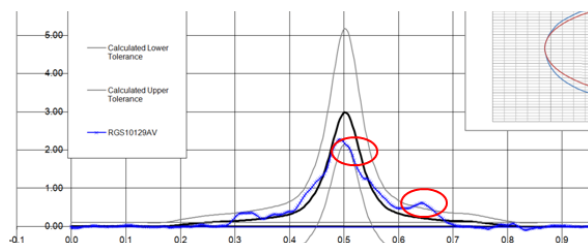
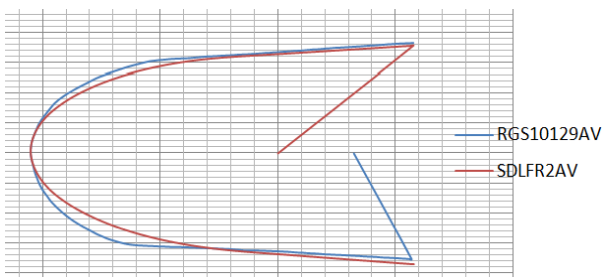
$$R=1/K$$

The radii range for the above population was found to be 0.1 mm. There will be some uncertainty associated with such a value due to the smoothing parameters used during the curvature averaging step in the software analysis.

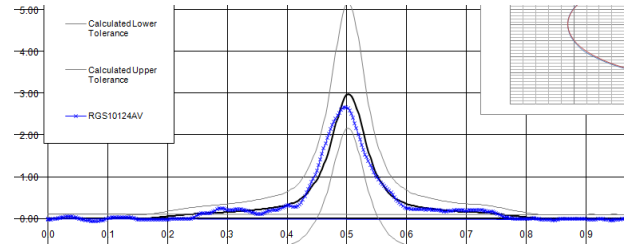
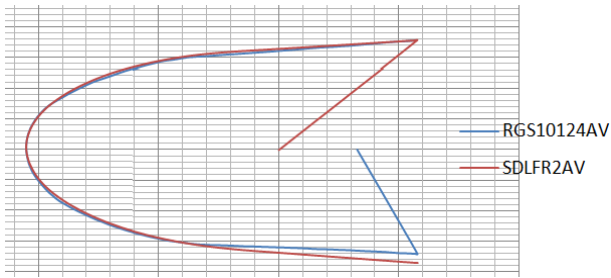
Although no tolerance bands have been derived for this method it is clear that certain non-desirable features could be identified from the curvature plot. The two plots below show examples of such features and how these could be captured using the CVALUTL method. Both Figures 13 a) and b) deviated from the nominal profile defined by the section AV. Figure c) followed the nominal profile. The deviations observed on the a) and b) leading edge profiles could also be seen on the curvature plots. It is also clear that the peak curvature for the a) and b) profiles is lower than the peak curvature of profile c).



a)



b)



c) **Figure 7. a),b) Leading edges with possible undesirable features ; c) Leading edge with very good profile**

As previously described in section 4.1 there were two modes of operation available in BI. This section describes how both modes affected the second method available for leading edge assessment. The method of plotting curvature vs the thickness line defined during the analysis was originally selected as the preferred method. This section describes testing done for this method using the same data from section 4.1.

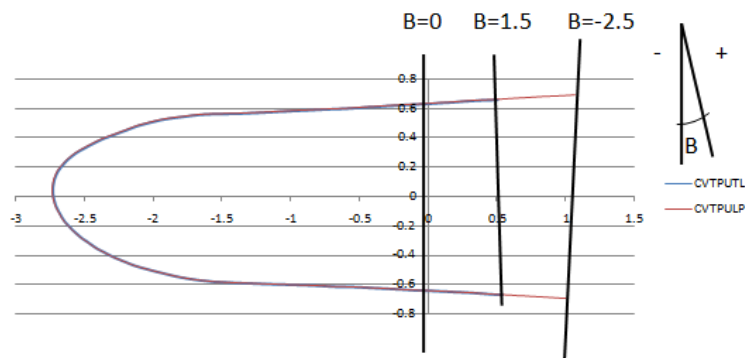


**Figure 8. Change in angle with start positing for the analysis.**

From the plot above it was found that the CVTPULP mode caused a shift of the curvature plot when compared to CVTPUTL mode. There were two variables responsible for such shift. The angle between the first and last points of the thickness lines were found to be -2.6 degrees for the LP mode and 1.5 degrees in TL mode. The difference found caused the curvature plots to shift in the X axis. Although the angle difference was the main cause for the shift in the curvature plot, the fact that TL mode and LP mode were at a distance X from each other also added to the shift in the curvature plot.

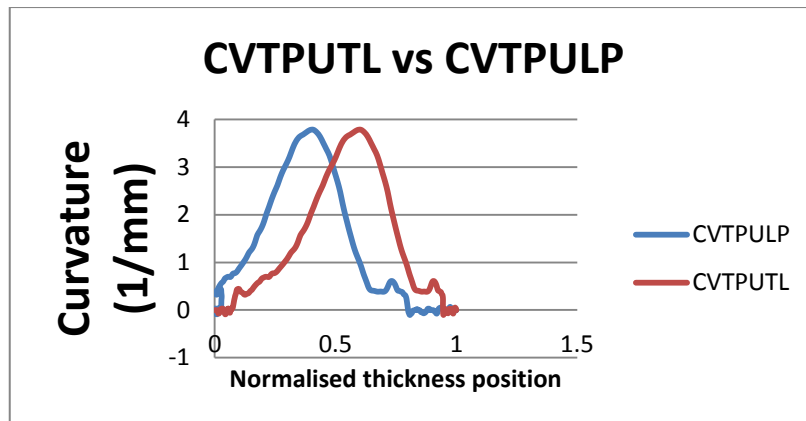


**Figure 9. Shift in curvature plots due to change in angle at the start position of the analysis.**

A set of Rotor2 blades were assessed using the same method as presented in section 3 of this document. Because Rotor2 airfoils were thinner, this caused the curvature plots to expand along the X axis. This variable is essentially a scaling effect i.e the difference between thicknesses for a set of blades. From the 140 sections analysed for Rotor2 data only 32 were accepted with the current tolerance band settings. It was also found that the thinner sections AY and AZ had the highest rejection rate.

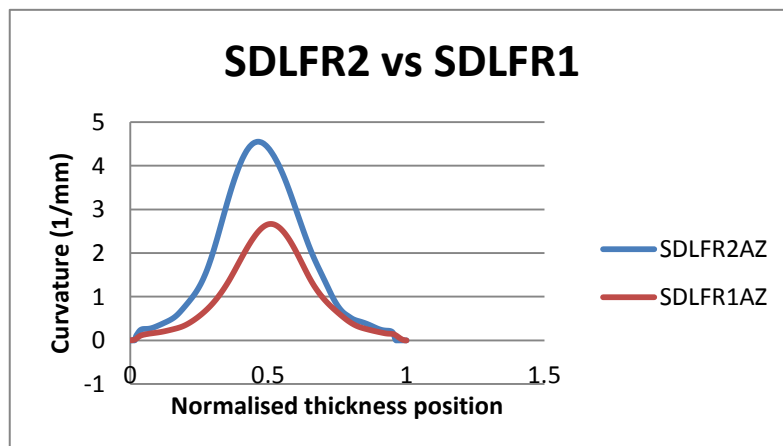


**Figure 10. Difference in curvature between first and last section of a blade airfoil.**

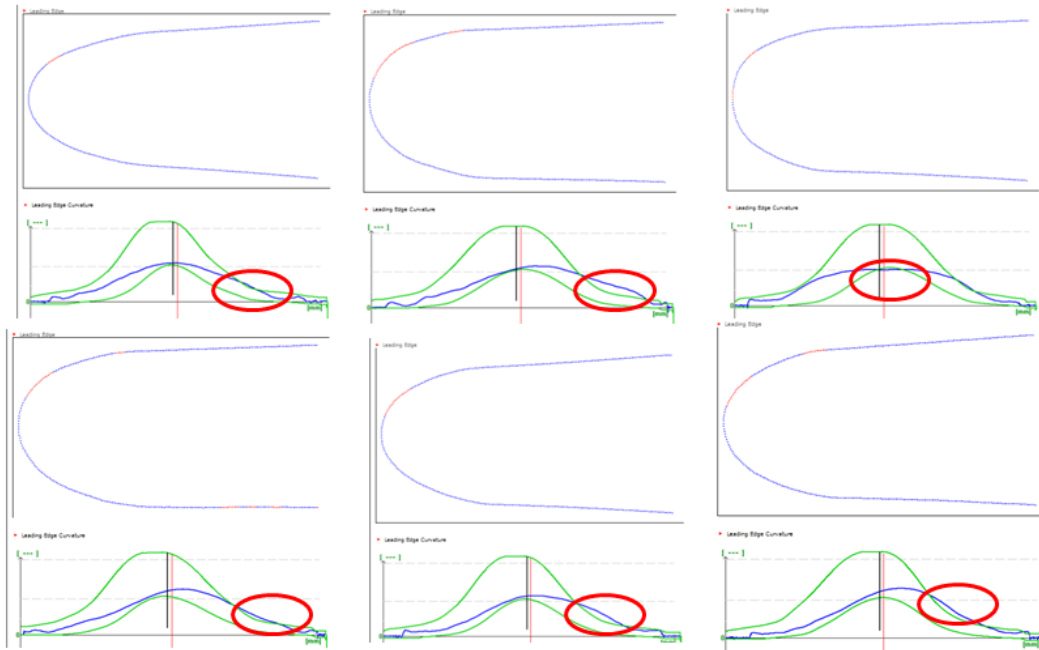


**Figure 11. Blade inspect Tolerancing method assessment of rotor2 blades.**

## 4.5 Conclusions

Two possible methods for the automated assessment of airfoil leading edge shape were assessed in this document. In both methods there were two modes available:

- 1 – A defined distance back from the leading edge tip
- 2 – Using last points on the point cloud data

The CVNTP method tests revealed that for Rotor1 airfoils, the method was stable enough due to magnitude of the thickness of the leading edges. When the same method was applied to Rotor2 data, it was found that the rejection rate was higher when compared with Rotor1 data. While for Rotor1 a simple adjustment of the tolerance bends would improve the performance of the CVTP method, for Rotor2 a different approach may be required given the results obtained. These results were obtained using mode 1.

The CVNAL method overcame some of the variation observed in the CVTP method due to the fact that curvature was being plotted against a bigger distance and therefore any uncertainty due to angle variations at the start point of the analysis could be considered negligible. This method showed some drawbacks such as the emphasis on the bias of the leading edge, which was clearly visible in the CVTP method. These results were obtained using mode 1.

For both methods testing revealed that although both modes of operation will have some uncertainty associated with them, using mode 1 will always provide more stability due to the set distance back from the leading edge. As this distance increases any minor angle change on the thickness line will be passed on as a shift in the X axis of the curvature plot.

Further work is required to identify a starting point for the tolerance bands using both methods.



UNIVERSITY OF BIRMINGHAM

# Measurement Technology

## Measurement Uncertainty in Coordinate Measuring Machines

Hugo Lobato EngD conference 27-28 February 2007

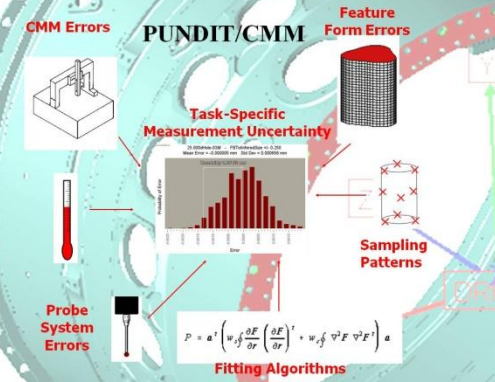
Industrial supervisor:  
Nick Orchard

### 1. Introduction

All measurement processes have some extent of uncertainty. The results of a measurement are therefore an approximated value of the quantity being reported. Coordinate measuring machines (CMMs) offer the versatility that is demanded by today's industry. Despite their known advantages over conventional measuring devices its performance is limited by several factors. Quantifying the contribution of each of the factors to the machine's measurement uncertainty is a non-trivial task. CMMs tend to be used at the final stage of a production process. Its results will govern the statistical process control for a product. Process capability will therefore be influenced by both the manufacturing stage and the inspection stage. Quantifying how much the measurement process is contributing to the process variability is key to understand all other variables in the process. Guides such as the GUM [1] provide a methodology to build uncertainty budgets. It breaks down all the standard uncertainties into type A or type B. Equation 1 is then used to combine all standard uncertainties in quadrature

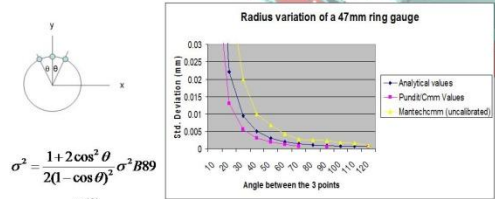
$$u_c^2(y) = \sum_{i=1}^N \left( \frac{\partial f}{\partial x_i} \right)^2 u^2(x_i) \quad \text{eq(1)}$$

Determining standard uncertainties for each machine on a production line can be a daunting and time consuming task. Thermal errors [2] are known to be one of the most important factors that affect the CMM measurement uncertainty. Quantifying such thermal effects would involve several experiments and good control of the temperature surrounding the machine which in some cases is not possible. Combining this effect with the fact that every machine will have different rigid body errors makes determining task specific measurement uncertainty very difficult. Another approach for determining CMM measurement uncertainty is provided by the ISO/TS 15530-3. Although this approach is easier, it still involves experimental designs where each factors needs to be controlled in a stable condition in order to quantify its effect. **A new approach to CMM measurement uncertainty is the use of computer (Monte Carlo) techniques.** Such simulation methods offer the advantage of highly detailed and advanced mathematical models of CMM error propagation that can be easily configured to the specific measurement task under consideration.



### 2. Evaluation

Measurement of a calibrated ring gauge. Using the standard deviation ( $\sigma$ ) of the probe calibration procedure and applying it to equation [3] 2 provides standard deviation of CMM measurements. Graph 1 shows the comparison between Pundit results and CMM.



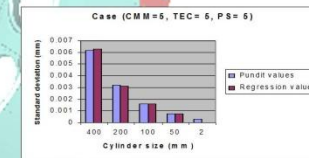
Graph 1. Comparison of the standard deviation between the CMM, Analytical values and Pundit.

$$\sigma^2 = \frac{1 + 2 \cos^2 \theta}{2(1 - \cos \theta)^2} \sigma^2 B89 \quad \text{eq(2)}$$

### 3. Applications

Used Pundit to populate Minitab design of experiments (DOE). Build regression models for measurement of specific features. The variables x,y,w and z refer to the coefficients of the regression equation (3). Graph 2 shows the regression model has very low errors.

$$SD = \frac{n}{2} \times \frac{x1}{n/2} \times \frac{x2}{n/2} \times x2 + \frac{y2}{n/2} \times \left( \frac{y1}{n/2} \right) + \frac{n}{2} \times \frac{w1}{n/2} \times \frac{w2}{n/2} \times w2 + \frac{z2}{n/2} \times \left( \frac{z1}{n/2} \right) \quad \text{eq(3)}$$



Graph 2. Regression model errors for a specific experiment in the DOE

### 4. Conclusions

The evaluation of Pundit/CMM indicates that there are no serious errors within the software. It is important to stress that the way the rigid body errors are generated does not necessarily represents a specific machine but a population of machines. This can affect the software performance if one is to use the software for a specific machine rather than a population. The potential of the software as a DOE tool for estimating task specific measurement uncertainty was shown and regression models developed. The next stage of research will include comparison between a real DOE and Pundit. This will provide insight in to the software behaviour trends.

[1]GUM, Guide to the estimation of Uncertainty in Measurement  
 [2] Valdés, R., A.Di Giacomo, B.Paziani, F. T., Synthesization of thermally induced errors in coordinate measuring machines, Journal of the Brazilian Society of Mechanical Sciences and Engineering, Vol. XXVII, No. 2, April-June 2005  
 [3] T. H. Hopp, The sensitivity of three-point circle fitting, NISTIR 5501 (1994)



Rolls-Royce



# Measurement Technology

## Measurement Uncertainty in Coordinate Measuring Machines Automated assessment of airfoil profiles

Hugo Lobato

EngD conference 5-6 March 2008

Academic supervisor:  
**Prof. Paul Maropoulos**  
(Bath University)

Industrial supervisor:  
**Nick Orchard**  
(Rolls-Royce)

### 1. Measurement Uncertainty in Coordinate measuring machines

All measurement processes have some extent of uncertainty. The results of a measurement are therefore an approximated value of the quantity being reported. Coordinate measuring machines (CMMs) offer the versatility that is demanded by today's industry. Despite their known advantages over conventional measuring devices its performance is dependent on several factors. Quantifying the contribution of each of the factors to the machine's measurement uncertainty is a non-trivial task. In this work, the uncertainty of CMM measurements is estimated by a single parameter (*rms*) accounting for both systematic and random errors:

$$rms(\bar{x}, \theta, n) = \sqrt{\frac{\sum_{i=1}^n (\bar{x}_i - \bar{x})^2}{n} + \frac{\sum_{i=1}^n (x_i - \theta)^2}{n}} \quad \text{eq (1)}$$

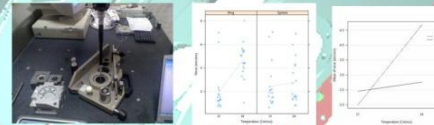
Factors such as environmental conditions (temperature), discretionary set-up parameters (probe extension, stylus length) and measuring plan decisions (number of points) are summarised in table-1.

FACTORS	LABELS	LEVELS
Room temperature (°C)	$temp_{(j)}$ $j = 1, \dots, 72$	20 24
Feature	$fea_{(j)}$ $j = 1, \dots, 72$	Ring (R) Sphere (S)
Probe extension (mm)	$pe_{(j)}$ $j = 1, \dots, 72$	0 100 200
Stylus length (mm)	$sl_{(j)}$ $j = 1, \dots, 72$	20 60 110
No. of probing points	$np_{(j)}$ $j = 1, \dots, 72$	7 11

Table-1. CMM factors

A model was fitted to the experimental data using the ordinary least squares method (OLS) as implemented in R [1]. A large number of two-way interactions were found not to be statistically significant resulting in the following final model:

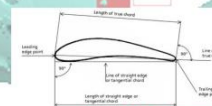
$$\log(\hat{rms}_j) = \mu + temp_{(j)} + fea_{(j)} + pe_{(j)} + sl_{(j)} + np_{(j)} + temp_{(j)} : fea_{(j)} + pe_{(j)} : sl_{(j)} + fea_{(j)} : np_{(j)} + er_j \quad \text{eq (2)}$$



The results obtained show that the *rms* value for the ring features increased with increment in temperature while the *rms* value for the sphere feature remained constant. This result is also supported by the interaction of feature type and temperature.

### 2. Automated assessment of airfoil profiles

Airfoil profiles are one of the most important features in the compressor stages of a gas turbine engine. Existing inspection methods of these features rely to a large extent on visual assessment. Leading edge airfoil shape is of significant importance but difficult to evaluate due to its free form nature.



A novel approach to the assessment of leading edge shape using curvature assessment was developed. A B-Spline was used to define the leading edge shape using coordinate data supplied by a measurement system.

$$P(t) = S_{i=0:n} N_{i,k}(t) P_i, \quad t_{k-1} < t < t_{k+1}$$

The resulting cubic polynomials ( $P_{n-1}$ ) can be used to derive the curvature  $K$  of the leading edge profile where  $K$ :

$$K = \frac{|x' \cdot y'' - x'' \cdot y'|}{(x'^2 + y'^2)^{3/2}} = \frac{|y''}{(1 + y'^2)^{3/2}}$$

Used Pundit to populate Minitab design of experiments (DOE). Build regression models for measurement of specific features. The variables *x*, *y*, *w* and *z* refer to the coefficients of the regression equation (3). Graph 2 shows the regression model has very low errors.

### 4. Conclusions

The evaluation of Pundit/CMM indicates that there are no serious errors within the software. It is important to stress that the way the rigid body errors are generated does not necessarily represent a specific machine but a population of machines. This can affect the software performance if one is to use the software for a specific machine rather than a population. The potential of the software as a DOE tool for estimating task specific measurement uncertainty was shown and regression models developed. The next stage of research will include comparison between a real DOE and Pundit. This will provide insight in to the software behaviour trends.

[1] GUM, Guide to the estimation of Uncertainty in Measurement  
 [2] Valdés, R., A. Di Giacomo, B. Pazian, F. T., Synthesis of thermally induced errors in coordinate measuring machines, Journal of the Brazilian Society of Mechanical Sciences and Engineering, Vol. XXVII, No. 2, April-June 2005  
 [3] T. H. Hopp, The sensitivity of three-point circle fitting, NISTIR 5501 (1994)



Rolls-Royce



## Appendix 6 – Engineering Doctorate Timeline

